NTNU – Trondheim
Norwegian University of
Science and Technology

Speed Observers for Mechanical Systems and Vehicles

Tine Charlotte Sundt

Master of Science in Engineering Cybernetics
Submission date: June 2012
Supervisor: Ole Morten Aamo, ITK

Norwegian University of Science and Technology
Department of Engineering Cybernetics

NTNU
Norges teknisk-naturvitenskapelige universitet

Fakultet for informasjonsteknologi, matematikk og elektroteknikk

Institutt for teknisk kybernetikk

HOVEDOPPGAVE

Kandidatens navn: Tine Charlotte Sundt

Fag: Teknisk Kybernetikk

Oppgavens tittel: Hastighetsestimering for mekaniske systemer og fartøy

-

Bakgrunn

Når man skal styre mekaniske systemer, har man vanligvis ikke hastighetsmålinger tilgjengelig direkte. Man må da ty til tilstandsestimering basert på posisjonsmålinger. Det har opp gjennom årenes løp vært stor aktivitet omkring slik estimering og spesielt har man manglet estimatorer med konvergensegenskaper som holder globalt. I [1] ble det presentert en estimator med globale konvergensegenskaper, mens i [2] ble en estimator med semi-globale egenskaper anvendt. Formålet med denne oppgaven er å sammenligne ytelsen til disse to på et gitt system.

Oppgave:

1) Gjør et litteraturstudie av ulineære tilstandsestimatorer for estimering av hastighet i mekaniske systemer.
2) Undersøk muligheten for anvendelse av resultatene i [1] på skipsmodellen i [2].
3) Simuler både ny løsning og løsningen fra [2] i MATLAB/SIMULINK og sammenlign.
4) Diskuter styrker og svakheter ved de to estimatorene. Vanskelig å tune? Tåler de støy? Osv.
5) Skriv rapport.

Faglærer/Veileder: Professor Ole Morten Aamo

[1] Stamnes, Aamo, and Kaasa, «A constructive speed observer design for general Euler-Lagrange systems», Automatica, vol.47, pp. 2233-2238, 2011.
[2] Wondergem, Lefeber, Pettersen, and Nijmeijer, «Output feedback tracking of ships », IEEE Transactions on Control Systems Technology, vol. 19, no. 2, 2011.

Abstract

The velocity observer in Wondergem et al. [2011] (*the Wondergem Observer*) and the velocity observer in Øyvind Nistad Stamnes et al. [2011] (*the Stamnes Observer*) are evaluated and compared for a ship model given in Wondergem et al. [2011]. The former observer has shown to be uniformly semi-globally exponentially stable. The latter observer has proven to be uniformly globally asymptotically stable and semi-globally exponentially stable when certain requirements are satisfied. However, due to a non-linear damping term in the ship model, the Stamnes Observer only meets the conditions for uniformly semi-globally exponentially stability.

The two observers have shown different convergence properties. The Wondergem Observer has a large overshoot during the settling period, then follows the reference robustly. The Stamnes Observer has a first order system behaviour and can become underdamped in the position convergence. Both observers show similar behaviour when considering a bias in the system equations. However, the run time for the Stamnes observer when simulating on a desktop computer is one to two orders of magnitude longer than for the Wondergem Observer.

From the evaluations in this thesis, the Wondergem Observer has shown to be the best choice for the given ship model. It is more robust than the Stamnes Observer, it does not have a lower degree of stability as first implied, and it has a much simpler structure.

Sammendrag

The following is a Norwegian version of the abstract.

Hastighetsestimatoren i Øyvind Nistad Stamnes et al. [2011] (*Stamnes-estimatoren*) og hastighetsestimatoren i Wondergem et al. [2011] (*Wondergem-estimatoren*) er sammenlignet og evaluert for skipsmodellen presentert i Wondergem et al. [2011]. Wondergem-estimatoren har i artikkelen bevist å ha uniform global asymptotisk stabilitet, og semi-global eksponensiell stabilitet, men når den anvendes for skipsmodellen ble ikke alle betingelsene for global stabilitet oppfylt. Den er likevel bevist til å ha uniform semi-global eksponensiell stabilitet, noe som fører at de to estimatorene har like høy grad av stabilitet.

De to estimatorene har ulike konvergensegenskaper. Wondergem-estimatoren har vist seg å få oversving i innsvingningsperioden, men følger referansen robust etter at den har konvergert. Stamnes-estimatoren har oppførsel som et førsteordens system, og får derfor en underdempet konvergensoppførsel i posisjonsestimatet. Begge estimatorene viser liknende oppførsel når unøyaktigheter er lagt til i systemlikningene. Kjøretiden for Stamnes-estimatoren når det simuleres på en PC er en til to størrelsesordener større enn for Wondergem-estimatoren.

Basert på evalueringene i denne oppgaven viser det seg at Wondergem-estimatoren er det beste valget for skipsmodellen. Den er mer robust enn Stamnes-estimatoren, den har ikke lavere grad av stabilitet enn Stamnes-estimatoren som først antatt, og den har en enklere struktur som gjør den lettere å jobbe med.

Acknowledgements

I wish to express my appreciation to my supervisor Ole Morten Aamo for his support and help during the Master's thesis, and for our valuable discussions regarding both the thesis as a whole and the implementation of the observer dynamics. I would also thank Stian Søvik, Ragnhild Holmvik and Ellen Lycke for helping me proofreading the thesis. I would also thank the people at the UAV-lab for a positive and helpful working environment.

Contents

List of Figures

List of Abbreviations

DGPS Differential Global Positioning Systen

DOF Degrees Of Freedom

DP Dynamic Positioning

GUAS Global Uniformly Asymptotic Stability

NED North East Down

Chapter 1

Introduction

1.1 Motivation

For control purposes, it is often critical to know the velocity of a mechanical system, such as a ship. For most ships, only the position and orientation measurements are available, or the velocity measurement contains an excessive amount of noise, so that it is not accurate enough to be used in a control scheme. However, based on measurements of position and orientation together with a model of the ship dynamics and the input vector, it is possible to calculate an accurate estimate of the velocity using an observer.

The ship position is usually measured by a Navstar Differential Global Positioning System (DGPS), and the orientation is measured using a gyro compass (Fossen [2011]). When using these measurements, the observer calculates a velocity estimate that is accurate enough to be used in a feedback control of the ship.

Important properties for observers are global convergence, stability, how easy it is to implement for a system, and robustness. Using a non-linear observer for a non-linear system, gives the advantage that it is possible to obtain a globally stable result without linearising the system (Wondergem et al. [2011]).

In this thesis, the goal is to compare the performance of two non-linear speed observers implemented for a ship model found in Wondergem et al. [2011]. The first observer, presented in Øyvind Nistad Stamnes et al. [2011], proves the existence of a globally exponentially convergent speed observer for Euler-Lagrange systems with a constructive design that solves the speed observer problem with equations on closed form. The second observer, presented in Wondergem et al. [2011], has proven to have semi-global uniform exponential stability of the closed-loop system.

1.2 Previous Work

Due to the importance of speed observers, many scientists have researched this topic, coming up with both linear and non-linear observers with different properties and limitations. For non-linear observers, the property of global exponential stability has been important.

In conventional control systems for ships, a linearisation around 36 constant yaw angles separated by 10 degrees is made. The estimation is solved by computing a linear Kalman filter and feedback control gains for each of these linearised models. A drawback with this method is that the amount of parameters makes the estimator difficult and time-consuming to tune. Also, it can be difficult to relate the tuning parameters to physical quantities, causing an ad-hoc tuning procedure which does not guarantee the desired stability and convergence properties (Fossen [2011]).

An alternative to the conventional method is the non-linear observer. The motivation for using a non-linear observer is mainly to avoid linearising the system and to be able to formally prove a global stable result. Also, less extensive tuning is an advantage.

Non-linear observers were first applied to station-keeping of ships and rigs in Dynamic Positioning systems (DP) (Fossen [2011]). For systems with a velocity close to zero, an assumption can be made that the Coriolis and centripetal terms can be ignored. The non-linear observers have been further developed to be valid for general Euler-Lagrangian systems with Coriolis and centripetal acceleration, and later also expanded to handle

non-linear damping. Finally, observers were both non-linear damping, and Coriolis and centripetal terms are taken into account, have been designed.

In Aamo et al. [2000], a non-linear observer for an Euler-Lagrange system with non-linear damping is designed. The article shows that if the damping holds the property of monotone damping and also is locally Lipschitz, then the observer-controller system is globally uniformly asymptotically stable (GUAS). However, the property of monotone damping is rarely present in a marine system. Also, note that the system presented in this article does not include a Coriolis and centripetal term.

In both Skjetne and Shim [2001] and Pettersen and Nijmeijer [1999], a system with Coriolis and centripetal forces and moments, and linear damping in velocity is considered. In Pettersen and Nijmeijer [1999], an observer-controller system designed using a passivity based approach is presented. The idea behind passivity based control is to use feedback to transform the systems' natural energy to reach the control objective. This way, the passivity properties in closed loop are preserved. The error dynamics are proven to be semi-globally exponentially stable.

Combining these results, Wondergem et al. [2011] designs a non-linear observer considering both Coriolis and centripetal forces and moments, and non-linear damping for a dynamic ship model. The observer obtains semi-global stability for the closed system by applying the use of the properties of the Coriolis and centripetal forces and moments.

For mechanical systems, a non-linear globally exponentially convergent speed observer is proposed in Astolfi et al. [2009] and further developed to mechanical systems with non-holonomic constraints in Astolfi et al. [2010]. The immersion and invariance procedure from Astolfi et al. [2008] is used in both, in order to construct the speed observer in which the observer is transformed into a system with desired properties. A manifold is defined such that it is attractive and that the unmeasurable part of the state can be reconstructed from the function that defines the manifold (Astolfi et al. [2009]). However, these methods require solutions to certain integrals that cannot be guaranteed a priori.

In Øyvind Nistad Stamnes et al. [2011] ideas from Astolfi et al. [2010] are used to derive a uniformly globally asymptotically stable and semi-globally

exponentially stable velocity observer for mechanical systems. The system from Astolfi et al. [2010] is simplified and the number of states is reduced. Also, the integrations needed in Astolfi et al. [2010] are avoided in Øyvind Nistad Stamnes et al. [2011].

The Observers developed in Øyvind Nistad Stamnes et al. [2011] and Wondergem et al. [2011] are further explored in this thesis when implemented for the ship model in Wondergem et al. [2011]. Both articles are further elaborated in chapter 3.

1.3 Structure of the Thesis

After this introductory chapter, Chapter 2 gives a short preliminary on the most important notations and definitions. Chapter 3 gives a brief explanation of the ship model and the two observers used in this thesis. A discussion regarding implementation and tuning including an analysis of whether the Stamnes observer can be used on the ship model is given in Chapter 4. The simulation results and comparisons are then presented in Chapter 5. Finally, the conclusion and a section of recommended further work is given.

Chapter 2

Preliminaries

2.1 Notation and Definitions

In this section, the notation and definitions used in this thesis are presented. The Euclidean space of dimensions n will be denoted as $\mathbb{R}^n$ and the set of non-negative real values as $\mathbb{R}^+$. Matrices are denoted with a bold upper-case letter. The estimates are denoted by a hat, for example $\hat{x}$. The time derivative of a vector $x(t) \in \mathbb{R}^n$ is denoted with a dot, as $\dot{x}, \ddot{x}, ..., x^{(i)}$. The Euclidean norm $\|x\|_2 = (x^T x)^{1/2}$ for a vector x of dimension $\mathbb{R}^n$ and the induced matrix 2-norm, $\|\boldsymbol{A}\|_2 = \left[\lambda_{max}(\boldsymbol{A}^T\boldsymbol{A})\right]^{1/2}$, are denoted by $\|\cdot\|$. The smallest and largest eigenvalue of a matrix $\boldsymbol{A}$ are denoted $\lambda_{min}(\boldsymbol{A})$ and $\lambda_{max}(\boldsymbol{A})$, respectively. The determinant for a matrix $\boldsymbol{A}$ is denoted $det(\boldsymbol{A})$ and the adjoint is denoted $adj(\boldsymbol{A})$.

Forward Completeness

A system,

$$\dot{x} = f(x, \omega), \tag{2.1}$$

is forward complete, if for every initial condition and every measurable locally essentially bounded input signal ω, the solution is defined for all $t \leq 0$, i.e $T_{max} = +\infty$ (Krstic [2009]).

Existence of the Inverse

The inverse $\boldsymbol{A}^{-1}$ of an $n \times n$ matrix $\boldsymbol{A}$ exists if and only if $rank(\boldsymbol{A}) = n$, thus if and only if $det(\boldsymbol{A}) \neq 0$. Hence $\boldsymbol{A}$ is nonsingular if $rank(\boldsymbol{A}) = n$ and is singular if $rank(\boldsymbol{A}) < n$ (Kreyszig [2006]).

Inverse of a Matrix

The inverse of a nonsingular square matrix $\boldsymbol{A}$ is defined as (**?**):

$$\boldsymbol{A}^{-1} = \frac{adj(\boldsymbol{A})}{det(\boldsymbol{A})} \tag{2.2}$$

Scew Symetric

A matrix $\boldsymbol{S} \in SS(n)$, that is the set of skew-symmetric matrices of order n, is said to be skew-symetrical if:

$$\boldsymbol{S}(y, x) = -\boldsymbol{S}^T(y, x). \tag{2.3}$$

This implies that the off-diagonal elements of $\boldsymbol{S}$ satisfy $s_{ij} = -s_{ji}$ for $i \neq j$ while the diagonal elements are zero (Fossen [2011]).

Linear Transformation

Linearity or a linear transformation has the definition (Stacey [2010]):
Let $\boldsymbol{V}$ and $\boldsymbol{W}$ be vector spaces, a function $\boldsymbol{T} : \boldsymbol{V} \to \boldsymbol{W}$ is a linear transformation if for $u, v \in \boldsymbol{V}$ and $\lambda \in \mathbb{R}$

$$\boldsymbol{T}(0_{\boldsymbol{V}}) = 0_{\boldsymbol{W}}, \tag{2.4}$$

$$\boldsymbol{T}(u + v) = \boldsymbol{T}(u) + \boldsymbol{T}(v), \tag{2.5}$$

$$\boldsymbol{T}(\lambda v) = \lambda \boldsymbol{T}(v) \tag{2.6}$$

Semi-global Stability

A feedback system is semi-globally stable if the system does not achieve global stability, but can be designed such that any given compact set, can be included in the region of attraction (Khalil [2002]).

Globally Uniformly Asymptotically Stable

Let $x = 0$ be an equilibrium point for a function

$$\dot{x} = f(t, x), \tag{2.7}$$

and $D \subset R^n$ be a domain containing $x = 0$. Let $V : [0, \infty) \times D \to R$ be a continuously differentiable function such that

$$W_1(x) \leq V(t, x) \leq W_2(x), \tag{2.8}$$

$$\frac{\partial V}{\partial t} + \frac{\partial V}{\partial x} f(t, x) \leq -W_3(x), \tag{2.9}$$

$\forall t \geq 0$ and $\forall x \in D$, where $W_1(x)$, $W_2(x)$ and $W_3(x)$ are continuous positive definite functions on D. Then $x = 0$ is uniformly asymptotically stable. Moreover, if r and c are chosen such that $B_r = \{\|x\| \leq r\} \subset D$ and $c < min_{\|x\|=r} W_1(x)$, then every trajectory starting in $\{x \in B_r | W_2(x) \leq c\}$ satisfies

$$\|x(t)\| \leq \beta(\|x(t_0)\|, t - t_0), \forall t \geq t_0 \geq 0 \tag{2.10}$$

for some class $\mathcal{KL}$ function β. Finally, if $D = R^n$ and $W_1(x)$ is radially unbounded, then $x = 0$ is globally uniformly asymptotically stable (Khalil [2002]).

Semi-Globally Uniformly Exponentially Stability

The equilibrium point $x = 0$ is said to be semi-globally uniform exponential stable if for each $r > 0$ and for all $(t_0, x(t_0)) \in \mathbb{R}^+ \times \mathcal{B}$, a function $\beta \in \mathcal{KL}$ exists such that

$$\|x(t)\| \leq \beta(\|x(t_0)\|, t - t_0), \forall t \geq t_0 \geq 0, \forall x(t_0) \in \mathcal{B}_r \tag{2.11}$$

where β

$$\beta = k\|x(t_0)\|exp^{-\gamma(t-t_0)}k > 0, \gamma > 0 \tag{2.12}$$

(Wondergem et al. [2009])

2.2 Froude Scaling

Froude scaling is a dimensionless number defined as the ratio of channel velocity to the speed of propagation of a small-disturbance wave in an open channel (White [2003]). It is used to determine the resistance of a partially submerged body, and can be used to compare objects of different sizes. The froude number is determined by

$$Fn := \frac{U}{\sqrt{gL}}, \tag{2.13}$$

where U is the maximum operating speed, L is the submerged length and g is the acceleration of gravity (Fossen [2011]).

If two vessels, a ship S and a model M, has the same froude number, then the scaling number λ_{Fr} is found from

$$\frac{U_M}{\sqrt{gL_M}} = \frac{U_S}{\sqrt{gL_S}}, \tag{2.14}$$

$$\frac{U_M}{U_S} = \frac{\sqrt{gL_M}}{\sqrt{gL_S}} = \sqrt{\lambda_{Fr}}. \tag{2.15}$$

Chapter 3

Ship Model and Observer Dynamics

There are different approaches to estimate the velocity of a mechanical system based on position measurements for a non-linear mechanical system. This chapter will briefly explain different state estimators for mechanical systems.

A simple, but very inaccurate observer, is the derivative of the position data. For systems with measurement noise, this approach can give very unsatisfying results. When differentiating a signal with high frequency measurement noise, the estimated velocity can deviate considerably from the real value, but most importantly, the noise is amplified.

By using a Kalman filter to estimate the velocity of the mechanical system, the noise is compensated for. However, tuning a Kalman filter is difficult and very time consuming (Fossen [2002]). This is due to the number of covariance tuning parameters that are difficult to relate to physical quantities. Also, global stability cannot be guaranteed analytically by using this method (Fossen [2002]). On the other hand, Kalman filters has a widespread use in the industry, and experiments show that it works very well. However, the scope of this thesis only includes methods where stability for the total system can be proven analytically.

3.1 Ship Model

In this section, the ship model used in this thesis is presented in a vectorial setting according to Fossen [1991]. It is a 3 degrees of freedom (3DOF) model and it is presented in an Earth-fixed frame that can be considered an inertial North East Down frame (NED-frame). Also, the transformation from the Body Fixed frame to NED is shown by the use of rotational matrices. The ship model is given by

$$\boldsymbol{M}(\eta)\ddot{\eta} + \boldsymbol{C}(\eta,\dot{\eta})\dot{\eta} + \boldsymbol{D}(\eta,\dot{\eta})\eta = \tau, \tag{3.1}$$

where $\boldsymbol{M}(\eta)$ is the inertia matrix including added mass, $\boldsymbol{C}(\eta,\dot{\eta})$ represents Coriolis and centripetal forces and moments, and $\boldsymbol{D}(\eta,\dot{\eta})$ is the damping matrix, containing both linear and non-linear damping terms (Fossen [1991]). The position vector has the notation $\eta = \begin{bmatrix} x & y & \psi \end{bmatrix}^T$, where x and y represent the position in respectively x (North) and y (East) direction, ψ represents the yaw angle. The vector $\tau \in \mathbb{R}^3$ is the vector of inputs.

The transformation of the system matrices from body to NED is done by

$$\boldsymbol{M}(\eta) = \boldsymbol{J}(\psi)\boldsymbol{M}\boldsymbol{J}^T(\psi) \tag{3.2}$$

$$\boldsymbol{C}(\eta,\dot{\eta}) = \boldsymbol{J}(\psi)\left(\boldsymbol{C}(\boldsymbol{J}^T(\psi)\dot{\eta}) - \boldsymbol{M}\boldsymbol{S}(\dot{\psi})\right)\boldsymbol{J}^T(\psi) \tag{3.3}$$

$$\boldsymbol{D}(\eta,\dot{\eta}) = \boldsymbol{J}(\psi)\boldsymbol{D}(\boldsymbol{J}^T(\psi)\dot{\eta})\boldsymbol{J}^T(\psi), \tag{3.4}$$

where

$$\boldsymbol{J}(\psi) = \begin{bmatrix} \cos\psi & -\sin\psi & 0 \\ \sin\psi & \cos\psi & 0 \\ 0 & 0 & 1 \end{bmatrix}, \tag{3.5}$$

and

$$\boldsymbol{S}(\dot{\psi}) = \boldsymbol{S}(r) = \begin{bmatrix} 0 & -r & 0 \\ r & 0 & 0 \\ 0 & 0 & 0 \end{bmatrix}. \tag{3.6}$$

The vector $\dot{\eta}$ is found from $\dot{\eta} = \boldsymbol{J}(\psi)\nu$, where $\nu = \begin{bmatrix} u & v & r \end{bmatrix}^T \in \mathbb{R}^3$ and represents the velocity vector in the body frame. The elements u, v and

r is velocity in surge, sway and yaw, respectivly. $\boldsymbol{J}(\psi)$ is the rotational matrix, transforming the system form body to NED, and S is a skew symmetric matrix of the angular velocity, $\omega = \begin{bmatrix} p & q & r \end{bmatrix}$. The rotation in roll and pitch are not considered, which causes the first two elements in ω to be zero.

The model used, is from the supply ship model, "Cybership II". In the Body Fixed frame the model matrices of the non-linear manoeuvring model are defined as follows (Wondergem et al. [2011]):

$$\boldsymbol{M} = \begin{bmatrix} 25.8 & 0 & 0 \\ 0 & 33.8 & 1.0115 \\ 0 & 1.0115 & 2.76 \end{bmatrix}, \tag{3.7}$$

$$\boldsymbol{C}(\nu) = \begin{bmatrix} 0 & 0 & -33.8v - 1.0115r \\ 0 & 0 & 25.8u \\ 33.8v + 1.0115r & -25.8u & 0 \end{bmatrix}, \tag{3.8}$$

$$\boldsymbol{D}(\nu) = \begin{bmatrix} 0.72 + 1.33|u| & 0 & 0 \\ 0 & 0.86 + 36.28|v| & -0.11 \\ 0 & -0.11 - 5.04|v| & 0.5 \end{bmatrix}. \tag{3.9}$$

The ship model then satisfies the following four properties (Wondergem et al. [2011] and Wondergem et al. [2009]):

$$\boldsymbol{M}(\eta) = \boldsymbol{M}^T(\eta) > 0, \tag{3.10}$$

$$\boldsymbol{C}(q, x)y = \boldsymbol{C}(q, y)x, \ \forall x, y, \tag{3.11}$$

$$\|\boldsymbol{M}^{-1}(\eta)\| \leq M_M \ and \ \|\boldsymbol{C}(\eta, x)\| \leq C_M\|x\|, \ \forall \eta, x, \tag{3.12}$$

$$\dot{\boldsymbol{M}} = \boldsymbol{C} + \boldsymbol{C}^T. \tag{3.13}$$

The symmetry property in Equation 3.11 is based on the assumption that the vehicle is a conventional ship, and no high speed craft, and also on the assumption that the ship has starboard and port symmetries (Pettersen and Nijmeijer [1999]). The limits in Equation 3.12 are bounded in η, since $\boldsymbol{J}(\psi)$ is singular free (Wondergem et al. [2011]).

When considering physical limitations of the ship in Wondergem et al. [2011], an assumption $\|\dot{\eta}\| \leq V_M$ regarding limitations of the velocity can be made. Due to the fact that the different damping terms contribute to

both linear and quadratic damping, an additional assumption is made in Wondergem et al. [2011] that the total damping term satisfies

$$\|\boldsymbol{D}(q,x)x - \boldsymbol{D}(q,y)y\| \leq (d_{M1} + d_{M2}\|x-y\|)\|x-y\| \tag{3.14}$$

As mentioned previously, this ship model is based on the supply ship model "Cybership II", which has a Froude scale 1:70. The length is 1.3 m and the weight is 24 kg. The model has two screw-rudder pairs at the stern, and one two-blade tunnel thruster in the bow. The maximum actuated surge force, sway force and yaw moment is 2 N, 1.5 N and 1.5 Nm, respectively.

3.2 Observer Design

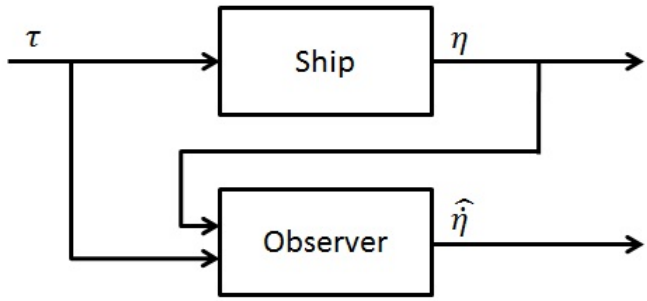

Figure 3.1: Ship-Observer System

This section contains a mathematical presentation of the speed observer in Wondergem et al. [2011], hereafter referred to as the Wondergem Observer, and the speed observer in Øyvind Nistad Stamnes et al. [2011], called the Stamnes observer. Both observers will be implemented and evaluated for the ship model presented in Section 3.1.

3.2.1 The Wondergem Observer

The observer in Wondergem et al. [2011] takes the complete ship dynamics into account, including both the Coriolis and centripetal forces and moments, and also the non-linear damping. This results, according to Wondergem et al. [2011], in a semi-globally uniformly stable closed loop system. The Lyapunov proof is given in Wondergem et al. [2009].

The observer equations as described in Wondergem et al. [2011][1]:

$$\dot{\hat{\eta}} = \hat{\dot{\eta}} + \boldsymbol{L}_1\tilde{\eta}, \tag{3.15}$$

$$\dot{\hat{\dot{\eta}}} = -\boldsymbol{M}^{-1}(\eta)\left[\boldsymbol{C}(\eta,\hat{\dot{\eta}})\hat{\dot{\eta}} + \boldsymbol{D}(\eta,\hat{\dot{\eta}})\hat{\dot{\eta}} - \tau\right] + \boldsymbol{L}_2\tilde{\eta}, \tag{3.16}$$

where $\hat{\dot{\eta}}$ is the estimate of the speed of the ship, the estimation bias is $\tilde{\eta} = \eta - \hat{\eta}$, the estimated position is $\hat{\eta}$. $\boldsymbol{M}(\eta)$, $\boldsymbol{C}(\eta,\hat{\dot{\eta}})$ and $\boldsymbol{D}(\eta,\hat{\dot{\eta}})$ refers to the system matrices from the ship model 3.1. $\boldsymbol{L}_1$ and $\boldsymbol{L}_2$ are tuning matrices that can be adjusted according to the error difference. They are chosen to be symmetric and positive definite. And at last the control vector, τ, is the input to the system.

Given $\hat{\eta}_0$ and $\hat{\dot{\eta}}_0$, the observer gains $\boldsymbol{L}_1$ and $\boldsymbol{L}_2$ are such that:

$$\lambda_{min}(\boldsymbol{L}_1) > 1, \lambda_{min}(\boldsymbol{L}_2) > 1, \tag{3.17}$$

$$\lambda_{min}(\boldsymbol{L}_2) > \frac{1}{2}M_M C_M V_M + \frac{1}{4}M_M d_{M1} V_M, \tag{3.18}$$

$$\lambda_{max}(\boldsymbol{L}_2) \geq \lambda_{min}(\boldsymbol{L}_2), \tag{3.19}$$

$$\lambda_{min}(\boldsymbol{L}_1) > \frac{(2\alpha_{11}+\gamma_2) + \sqrt{(2\alpha_{11}+\gamma_2)^2 - 4(2\alpha_{11}^2+\gamma_1)}}{2}, \tag{3.20}$$

$$\lambda_{max}(\boldsymbol{L}_1) \leq \frac{\lambda_{min}^2(\boldsymbol{L}_1) - 2\alpha_{11}\lambda_{min}(\boldsymbol{L}_1) + \alpha_{11}^2 - \gamma_1}{\gamma_2}, \tag{3.21}$$

where, as shown in Section 3.1, M_M, C_M, V_M are the upper bounds to $\boldsymbol{M}^{-1}(\eta)$, $\boldsymbol{C}(\eta,x)$ and the ship velocity $\dot{\eta}$. The terms d_{M1} and d_{M2} are

[1] Equation 3.16 differs from equation 3 in Wondergem et al. [2011] due to a sign error in Wondergem et al. [2011]

damping constants from Equation 3.14. The constants α_{11}, γ_1 and γ_2 are

$$\alpha_{11} = \frac{1}{2} + 3M_M C_M V_M + \frac{3}{2} M_M d_{M1} V_M, \tag{3.22}$$

$$\gamma_1 = (3M_M C_M + 3M_M d_{M2})^2 \left(\lambda_{max}(\boldsymbol{L}_2)\|\tilde{\eta}_0\|^2 + \|\dot{\tilde{\eta}}_0\|^2\right), \tag{3.23}$$

$$\gamma_2 = (3M_M C_M + 3M_M d_{M2})^2 \|\tilde{\eta}_0\|^2, \tag{3.24}$$

where

$$\tilde{\eta}_0 = \eta_0 - \hat{\eta}_0, \; \dot{\tilde{\eta}}_0 = \dot{\eta}_0 - \dot{\hat{\eta}}_0.$$

The proof of local uniform exponential stability of the observer error is found in Wondergem et al. [2009].

3.2.2 The Stamnes Observer

In this section, the Stamnes Observer is to be presented. The observer in Øyvind Nistad Stamnes et al. [2011] has been proven to be uniformly globally asymptotically stable and semi-globally exponentially stable when all the requirements explained below are satisfied. The observer is valid for Euler-Lagrangian systems that can be transformed into the the form:

$$\dot{y} = \boldsymbol{L}(y)x, \tag{3.25}$$

$$\dot{x} = \boldsymbol{S}(y,x)x + \boldsymbol{F}(y,x,u), \tag{3.26}$$

where $y \in \mathbb{R}^n$ and $x \in \mathbb{R}^{(n-k)}$. Here n is the dimension of the unmeasured velocity, and k is the number of constraints. The input u is such that the system is forward complete[2]. The system must satisfy the following conditions, as mentioned in the beginning of this section. $\boldsymbol{L}(y) \in \mathbb{R}^{n\times(n-k)}$ is required to be left-invertible, and both $\boldsymbol{L}(y)$ and $\boldsymbol{S}(y,x) \in \mathbb{R}^{(n-k)\times(n-k)}$ must be continuously differentiable. Also, $\boldsymbol{S}(y,x)$ is required to satisfy the properties of skew-symmetry and linearity in the second argument Astolfi et al. [2009]. $\boldsymbol{F}(x,y,u)$ must satisfy the sector condition: there exists a $c_F < \infty$ so that

$$[F(y,x,u) - F(y,\bar{x},u)]^T (x - \bar{x}) \leq c_F \|x - \bar{x}\|^2, \tag{3.27}$$

[2]Forward completeness is defined in Chapter 2.1

for the system to have global stability properties (Øyvind Nistad Stamnes et al. [2011]). This property is not guaranteed when using the Stamnes observer on the ship model. A further analysis is found in 4.2.

The observer equations from Øyvind Nistad Stamnes et al. [2011] are as follows:

$$\hat{x} = \xi + \boldsymbol{K}_x(\hat{\sigma}, \hat{y})y, \tag{3.28}$$

$$\dot{\hat{y}} = \boldsymbol{L}(y)\hat{x} + \boldsymbol{K}_y(y, \hat{y}, r, \hat{\sigma})\tilde{y}, \tag{3.29}$$

$$\dot{\xi} = \boldsymbol{S}(y, \hat{x})\hat{x} + \boldsymbol{F}(y, \hat{x}, u) - \boldsymbol{K}_x\boldsymbol{L}(y)\hat{x} - \frac{\partial \boldsymbol{K}_x}{\partial \hat{y}}\dot{\hat{y}}y - \frac{\partial \boldsymbol{K}_x}{\partial \hat{\sigma}}\dot{\hat{\sigma}}y, \tag{3.30}$$

$$\dot{r} = -\frac{\bar{k}_x}{2}(r - c_r) + r\left(\bar{\Delta}_y(y, \hat{y}, \hat{\sigma})\|\tilde{y}\| + \bar{\Delta}_\sigma(y, \hat{x}, \hat{\sigma})\|\tilde{\sigma}\|\right), \tag{3.31}$$

$$\dot{\hat{\sigma}} = Proj_{\hat{\sigma}}\left(2\left[\hat{x}^T\boldsymbol{F}(y, \hat{x}, u) + k_\sigma(y, \hat{y}, \hat{x}, r, \hat{\sigma}, \sigma)\tilde{\sigma}\right]\right), \tag{3.32}$$

where $\hat{y} \in \mathbb{R}^2$ and $\hat{x} \in \mathbb{R}^{n-k}$ are estimates of x and y. The estimation errors are defined as $\tilde{y} = y - \hat{y}$, $\tilde{x} = x - \hat{x}$ and $\tilde{\sigma} = \sigma - \hat{\sigma}$. The variable σ is defined as $\sigma = \|\hat{x}\|^2$. Both σ and r are added to dominate the Coriolis and centrifugal forces by using dynamic scaling. The design constant c_r affects the value of r, and by choosing c_r less than one, the sensitivity to measurement noise is reduced. However, the properties $c_r > 0$ and $r(t_0) \geq c_r$ must be fulfilled, and ensure that r stays larger than c_r and hence also larger than zero. The initial value $\hat{\sigma}_0$ must satisfy the property $\hat{\sigma}_0 \geq 0$. The gains $\boldsymbol{K}_x$, $\boldsymbol{K}_y$ and k_σ are defined as

$$\boldsymbol{K}_x(\hat{\sigma}, \hat{y}) = \left(\bar{k}_x + c_F + \varepsilon_y + \varepsilon_\sigma + c_s(\hat{y})\sqrt{1 + \hat{\sigma}}\right)\boldsymbol{L}^+(\hat{y}), \tag{3.33}$$

$$\boldsymbol{K}_y(y, \hat{y}, r, \hat{\sigma}) = \bar{k}_y\boldsymbol{I} + \frac{2r^2}{\bar{k}_x}\left(\|\boldsymbol{L}(y)\|^2 + \bar{\Delta}_y^2(y, \hat{y}, \hat{\sigma})\right)\boldsymbol{I}, \tag{3.34}$$

$$k_\sigma(y, \hat{y}, \hat{x}, r, \hat{\sigma}, \sigma) = \bar{k}_\sigma + \frac{2r^2}{\bar{k}_x}\left(\bar{\Delta}_\sigma^2(y, \sigma, \hat{\sigma}) + \|\hat{x}^T\boldsymbol{K}_x(\hat{\sigma}, \hat{y})\boldsymbol{L}(y)\|^2\right), \tag{3.35}$$

where

$$\bar{\Delta}_y(y,\hat{y},\hat{\sigma}) = \begin{cases} \frac{\Delta_y(y,\hat{y},\hat{\sigma})}{\|\tilde{y}\|} & \Delta_y(y,\hat{y},\hat{\sigma}) > \varepsilon_y \\ \frac{\Delta_y(y,\hat{y},\hat{\sigma})}{\|\Delta_y - \varepsilon_y\| + \|\tilde{y}\|} & else \end{cases} \tag{3.36}$$

$$\bar{\Delta}_\sigma(y,\sigma,\hat{\sigma}) = \begin{cases} \frac{\Delta_\sigma(y,\sigma,\hat{\sigma})}{\|\tilde{\sigma}\|} & \Delta_\sigma(y,\sigma,\hat{\sigma}) > \varepsilon_\sigma \\ \frac{\Delta_\sigma(y,\sigma,\hat{\sigma})}{\|\Delta_\sigma - \varepsilon_\sigma\| + \|\tilde{\sigma}\|} & else \end{cases} \tag{3.37}$$

$$\Delta_y(y,\hat{y},\hat{\sigma}) = \|c_s(y) - c_s(\hat{y})\|\sqrt{1+\hat{\sigma}} + \|\boldsymbol{K}_x(\hat{\sigma},\hat{y})\,(\boldsymbol{L}(y) - \boldsymbol{L}(\hat{y}))\| \tag{3.38}$$

$$\Delta_\sigma(y,\sigma,\hat{\sigma}) = c_s(y)\|\sqrt{1+\sigma} - \sqrt{1+\hat{\sigma}}\|. \tag{3.39}$$

Here, the matrices and variables defined above in equation3.33-3.39 are chosen to give a uniformly globally asymptotically stable and semi-globally exponentially stable result in the Lyapunov analysis shown in Øyvind Nistad Stamnes et al. [2011]. $\bar{k}_x > 0$, $\bar{k}_y > 0$ and $\bar{k}_\sigma > 0$ and can be used to increase convergence rates of the estimation errors (Øyvind Nistad Stamnes et al. [2011]). The stability results are summarized in the following theorem(Øyvind Nistad Stamnes et al. [2011]):

Theorem 3.2.1. *Suppose u is such that system (3.25-3.26) is forward complete, and consider the observer (3.28-3.39). There exists a strictly positive constant k and a continious function $\alpha(s) : \mathbb{R}^+ \to \mathbb{R}^+$ such that for any initial condition $y(t_0), \hat{y}(t_0) \in \mathbb{R}^n, x(t_0), \xi(t_0) \in \mathbb{R}^{n-k}, r(t_0) \geq c_r$ and $\hat{\sigma}(t_0) \geq 0$,*

$$\|\omega(t)\| \leq \alpha(\|\omega\|)e^{-k(t-t_0)}, \tag{3.40}$$

where $\omega = [\tilde{x}^T, \tilde{y}^T, \tilde{\sigma}, r - c_r]^T$.

The proof is found in Øyvind Nistad Stamnes et al. [2011].

Chapter 4

Analysis of the Observers

This chapter contains discussions and reflections considering the implementation and performance of the two observers presented in Chapter 3. In addition, a numerical analysis regarding the stability properties given in Øyvind Nistad Stamnes et al. [2011] is performed. Moreover, a transformation between the two observer systems are performed.

4.1 Transformation of the Ship Model

The Stamnes observer is designed for a system on the form in Equation 3.25 and 3.26, repeated below:

$$\begin{aligned} \dot{y} &= \boldsymbol{L}(y)x, \\ \dot{x} &= \boldsymbol{S}(y,x)x + \boldsymbol{F}(y,x,u). \end{aligned}$$

The ship model is given in on another form in Equation 3.1, repeated below:

$$\boldsymbol{M}(\eta)\ddot{\eta} + \boldsymbol{C}(\dot{\eta},\eta)\dot{\eta} + \boldsymbol{D}(\dot{\eta},\eta)\eta = \tau.$$

To transform the ship model into the form in Equation 3.25 and 3.26 so that the Stamnes observer can be used, the parameters have to be defined

as follows (Øyvind Nistad Stamnes et al. [2011])

$$y = \eta, x = \boldsymbol{T}(y)\dot{\eta} \tag{4.1}$$

The matrices $\boldsymbol{L}(y)$, $\boldsymbol{S}(y,x)$ and $\boldsymbol{F}(y,x,u)$ are defined as

$$\boldsymbol{L}(y) = \boldsymbol{T}^{-1}(y), \tag{4.2}$$

$$\boldsymbol{S}(y,x) = \left(\dot{\boldsymbol{T}}(y) - \boldsymbol{L}^T(y)\boldsymbol{C}(y,\boldsymbol{L}(y)x)\right)\boldsymbol{L}(y), \tag{4.3}$$

$$\boldsymbol{F}(x,y,u) = \boldsymbol{L}^T(y)\left(\boldsymbol{\tau} - \boldsymbol{D}(y,\boldsymbol{L}(y)x)\boldsymbol{L}(y)x\right), \tag{4.4}$$

where $\boldsymbol{T}$ is found from the Cholesky factorisation of $\boldsymbol{M}(y)$ as follows:

$$\boldsymbol{M}(y) = \boldsymbol{T}^T(y)\boldsymbol{T}(y). \tag{4.5}$$

This transformation is used to compare the two observers when implemented for the same ship model.

The mass matrix $\boldsymbol{M}(y)$ are found as follows:

$$\boldsymbol{M}(y) = \boldsymbol{J}(\psi)\boldsymbol{M}\boldsymbol{J}^T(\psi) = \tag{4.6}$$
$$\begin{bmatrix} 25.8cos^2(\psi) + 33.8sin^2(\psi) & -8sin(\psi)cos(\psi) & -1.0115sin(\psi) \\ -8sin(\psi)cos(\psi) & 25.8sin^2(\psi) + 33.8cos^2(\psi) & 1.0115cos(\psi) \\ -1.0115sin(\psi) & 1.0115cos(\psi) & 2.76 \end{bmatrix}.$$

Due to the complexity of $\boldsymbol{M}$, the Cholesky factorization of $\boldsymbol{M}$ gives a very complicated expression of $\boldsymbol{T}$. The inversion of $\boldsymbol{T}$ to find $\boldsymbol{L}$, and the derivation of $\boldsymbol{T}$ to find $\boldsymbol{S}$, gives matrices with elements of a very complicated trigonometric nature. Considering this fact, a direct implementation of the matrices $\boldsymbol{L}(y)$, $\boldsymbol{S}(y,x)$ and $\boldsymbol{F}(x,y,u)$ is not desirable in this case, and the implementation will therefore be done numerically. This is not optimal, and will increase the run time because of slow numerical functions in Matlab. In addition, the numerical approximations will make the simulation results less accurate. The Cholesky factorisation gives a unique solution (Kreyszig [2006]), which makes the numerical approach possible.

4.2 Analysis of the Stamnes Observer

This section contains an analysis of whether it is possible to use the Stamnes Observer for the ship model described in Section 3.1 such that

the theorem can be satisfied.

The first subject to be investigated is whether the ship model can be transformed to the form in equation 3.25 and 3.26. Recall the conditions that must be satisfied as mentioned in Section 3.2.2:

1. $\boldsymbol{L}(y) \in \mathbb{R}^{n\times(n-k)}$ is required to be left-invertible,
2. $\boldsymbol{L}(y)$ and $\boldsymbol{S}(y,x) \in \mathbb{R}^{(n-k)\times(n-k)}$ must be continuous differentiable,
3. $\boldsymbol{S}(y,x)$ satisfies the properties of skew-symmetry and linearity in the second argument, and
4. $\boldsymbol{F}(x,y,u)$ must satisfy the sector condition: there exists $c_F < \infty$ so that $[F(y,x,u) - F(y,\bar{x},u)]^T (x-\bar{x}) \leq c_F \|x-\bar{x}\|^2$.

The first condition to investigate is whether $\boldsymbol{L}(y)$ is a left invertible matrix. Recall from Chapter 2 that the existence of the inverse is defined as, for a $n \times n$ matrix; the inverse $\boldsymbol{A}^{-1}$ exists if and only if $rank(\boldsymbol{A}) = n$. Since $\boldsymbol{T}$, because of the Cholesky factorisation, is an upper triangular matrix, with non-zero elements on the diagonal, then $rank(\boldsymbol{T}) = n$ for all y. And since $\boldsymbol{T}$ is a non-singular invertible matrix, and $\boldsymbol{T}^{-1} = \boldsymbol{L}(y)$, a conclusion can be made that $\boldsymbol{L}(y)$ is a left-invertible matrix.

Condition 2 is valid if $\boldsymbol{L}(y)$ and $\boldsymbol{S}(y,x)$ are continuous differentiable. Since $\boldsymbol{M}$ is defined as continuous differentiable, $\boldsymbol{T}^T(y)\boldsymbol{T}(y)$ must also be continuous differentiable because of the equality in Equation 4.5. Hence, $\boldsymbol{T}$ must be continuous differentiable. Since $\boldsymbol{T}$ is a non-singular matrix from the paragraph above, then the determinant $det(\boldsymbol{T}(y)) \neq 0 \forall y$, and $\boldsymbol{T}$ is continuous differentiable, then also the inverse of $\boldsymbol{T}$, $\boldsymbol{L}(y)$, must be continuously differentiable by the properties of an inverse matrix (see Chapter 2). Since $\boldsymbol{T}$, $\boldsymbol{C}$ and $\boldsymbol{L}$ are continuous differentiable, then $\boldsymbol{S}$ must also be continuous differentiable by the definition of $\boldsymbol{S}$, recall that

$$\boldsymbol{S} = \left(\dot{\boldsymbol{T}} - \boldsymbol{T}^{-T}\boldsymbol{C}\right)\boldsymbol{T}^{-1}.$$

$\boldsymbol{S}$ is linear in the second argument by the definition of $\boldsymbol{S}$, in Equation 4.3 (Astolfi et al. [2009]). That follows from the linearity in $\boldsymbol{C}$ defined in Chapter 3.1. Since $\boldsymbol{C}$ is linear in the second argument and $\boldsymbol{T}$ is only dependent on the first argument, linearity can be concluded.

Skew-symmetry as defined in Chapter 2, is proven by Astolfi et al. [2009] in the following matter:

$$\begin{aligned}
\boldsymbol{S}+\boldsymbol{S}^T &= \dot{\boldsymbol{T}}\boldsymbol{T}^{-1}-\boldsymbol{T}^{-T}\boldsymbol{C}\boldsymbol{T}^{-1}+\boldsymbol{T}^{-T}\dot{\boldsymbol{T}}^T-\boldsymbol{T}^{-T}\boldsymbol{C}^T\boldsymbol{T}^{-1} \\
&= \dot{\boldsymbol{T}}\boldsymbol{T}^{-1}+\boldsymbol{T}^{-T}\dot{\boldsymbol{T}}^T-\boldsymbol{T}^{-T}(\boldsymbol{C}+\boldsymbol{C}^T)\boldsymbol{T}^{-1} \\
&= \dot{\boldsymbol{T}}\boldsymbol{T}^{-1}+\boldsymbol{T}^{-T}\dot{\boldsymbol{T}}^T-\boldsymbol{T}^{-T}\dot{\boldsymbol{M}}\boldsymbol{T}^{-1} \\
&= \dot{\boldsymbol{T}}\boldsymbol{T}^{-1}+\boldsymbol{T}^{-T}\dot{\boldsymbol{T}}^T-\boldsymbol{T}^{-T}(\dot{\boldsymbol{T}}^T\boldsymbol{T}+\boldsymbol{T}^T\dot{\boldsymbol{T}})\boldsymbol{T}^{-1} \\
&= 0.
\end{aligned}$$

When the other conditions are proven to be true, the last condition is crucial for the observer to be uniformly globally asymptotically stable and semi-globally exponentially stable. The investigation of the condition uses the definition of F given in Equation 4.4 as follows:

$$\begin{aligned}
\left[F(y,x,u)-F(y,\bar{x},u)\right]^T(x-\bar{x}) &= \\
\left[\boldsymbol{L}^T(y)\left(\boldsymbol{\tau}-\boldsymbol{D}(y,\boldsymbol{L}(y)x)\boldsymbol{L}(y)x\right)-\boldsymbol{L}^T(y)\left(\boldsymbol{\tau}-\boldsymbol{D}(y,\boldsymbol{L}(y)\bar{x})\boldsymbol{L}(y)\bar{x}\right)\right]^T(x-\bar{x}) &= \\
\left[\boldsymbol{D}(y,\boldsymbol{L}(y)\bar{x})\boldsymbol{L}(y)\bar{x}-\boldsymbol{D}(y,\boldsymbol{L}(y)x)\boldsymbol{L}(y)x\right]^T(x-\bar{x}) &\quad ,
\end{aligned}$$

which results in a third order term of x and $\hat{x}$, and therefore,

$$\left[F(y,x,u)-F(y,\bar{x},u)\right]^T(x-\bar{x}) \not\leq c_F\|x-\bar{x}\|^2,\ \forall x,\bar{x},y\ and\ \tau.$$

Hence, the sector condition is not proven to be true, for all $x, \bar{x}, y\ and\ \tau$. However, Condition 4 does hold for a subset of x and $\hat{x}$, which can be chosen arbitrarily large. Thus the system does not achieve globally stability, but can be designed such that for any given compact set of x and $\hat{x}$ a suficiently large c_F can be chosen such that Condition 4 is satisfied.

By the proof of Theorem 3.2.1 found in Øyvind Nistad Stamnes et al. [2011], a finite upper bound of the design variable r must be present for α to be linear, such that the observer is globally exponentially stable. As mentioned in Øyvind Nistad Stamnes et al. [2011], the upper bound of r is dependent on the initial values. However, by defining a compact space K of the initial values, an upper bound for r can be found, which is valid for all initial values in the space. Since K is compact, there exists a constant c such that $\|w\| < c,\ \forall w \in K$. Since α is continuous, there exists a constant $c_2 = sup(\alpha(q)), \forall q \in [0,c]$ which gives $\|\omega\| \leq \frac{c_2}{c}\|\omega_0\|e^{-k(t-t_0)}$.

For a given large compact subset of $x, \bar{x}$, a c_F can be found such that Condition 4 is true. Also, for a given compact space K of the initial values, Theorem 3.2.1 is shown to hold. Hence, semi-globally uniformly exponentially stability of the observer can be concluded.

4.3 Implementation and Tuning

Important factors in comparing the two observers, are stability properties, the ability to obtain an accurate estimation, and simplicity and robustness during both implementation and tuning. If a system is very complicated implementation-wise, errors are more likely to appear. On the other hand, a simpler system might lack the necessary accuracy.

Also, when tuning a system, the complexity can vary. If there are too many tuning parameters, the tuning can be very time consuming and difficult. However, if there are too few tuning parameters, a satisfying tuning to get a decent estimate, might not be achievable.

A reason for high complexity in a system is often the desire to prove a higher order of stability. For the Stamnes Observer this has been the case. In order to achieve global stability properties, the observer has attained complex structure. However, as shown in Section 4.2 only semi-global properties was proven for the Stamnes Observer when used on the ship model. When comparing with the Wondergem Observer which also has semi-global stability properties, the Stamnes Observer has unnecessary complexity for this case.

The Wondergem Observer has only two observer equations and two tuning matrices, making the implementation straight forward. However, achieving a critical damped behaviour for both the position estimate and the velocity estimate has shown to be difficult. When choosing a large gain, the overshoot quickly increases, and keeping the gain low causes an inaccurate and slow response. This behaviour is very common and the user must make a compromise. The general result of tuning is a second order system response.

The Stamnes observer consists of equations with dynamic gains. When

the observer estimates deviates largely from the reference value, the gains increases, and when the estimated value is close to the reference value, the gain decreases to make the observer less sensitive for measurement noise. The equations are complex, meaning that, many of the dynamic gains are used in the different elements in the equations. This leads to further implementation challenges, especially when debugging.

Also, the Stamnes Observer is very sensitive to changes in initial values regarding run time and convergence time for the simulation. When increasing the initial values, the run time increases, as is to be shown in Chapter 5. When increasing the design parameter r_0 described in Chapter 3.2.2, the amplification on the error between the estimated and the measured position in the first time step increases, causing the position estimate to converge quickly. However, the increase of r_0 also causes an increase in run time. Generally, when tuning the Stamnes Observer, it shows underdamped first order behaviour.

Moreover, the Stamnes Observer must do a large number of numerical operations for each time step during the simulation. This is because of the complexity of the equations as discussed in Section 4.1 and 4.2 which leads to the use of the Matlab functions *numjac* for numerical derivations and *chol* for Cholesky factorisations. Both functions are considered slow and can increase the run time.

An accurate estimation is crucial to be able to use the signal in a controller. Also a quick and robust tuning is desirable to avoid high maintenance. For the tuning chosen in this thesis, both observers converge to a neighbourhood around the true value, and follow the true value closely. The Wondergem Observer successfully can use the same tuning parameters for each case, unlike the Stamnes Observer that needs to adjust the tuning to be able to converge for the case with noise. This is mainly because of the considerations regarding run time. Without these considerations a more robust tuning for the Stamnes Observer would be desirable.

As proved in Wondergem et al. [2009], Section 4.2 and Øyvind Nistad Stamnes et al. [2011], both observers have proven to have semi-global uniform exponential stability when used for ship model. Hence, when implementing the system it is necessary to make sure the initial values are within the

stability region. A possibility is to make sure that the stability region covers the physical attainable values. An example is that it the stability region must include all velocities up to the ship's maximum velocity. For the Stamnes Observer, this can be done by choosing c_F large enough.

To summarise, the Stamnes Observer has a much more complex nature than the Wondergem Observer, causing the implementation to be more challenging for the former. Also, the Stamnes Observer generally shows a first order system behaviour, with underdamped convergence. The Wondergem Observer, on the other hand, shows a second order behaviour, where an overshoot is difficult to avoid by tuning. However, both observers obtain an accurate estimation after a short convergence time. Also, both observer semi-global uniform exponential stability. The user must therefore ensure that the stability region is sufficiently large.

Chapter 5

Simulation Results

The objective of this chapter is to present and discuss the results of the simulations of the equations described in Chapter 3 of the ship model and the observers.

In order to discuss the properties of the observers, they are first compared based on simulations without noise, then with measurement noise, and finally, when the observer ship model has inaccuracies in comparison to the real ship model. These cases have been chosen in order to test the observer in cases expected to be present on a real ship. Matlab 2010b is used to perform the simulations. The Matlab code is attached in a zip file available for the supervisor and external examiner at DAIM[1], and a quick start guide is to be found in Appendix A.

The ship model used in the simulations is shown in Section 3.1. It is transformed to the form shown in Equation 3.25 and 3.26, repeated below:

$$\begin{aligned} \dot{y} &= \boldsymbol{L}(y)x, \\ \dot{x} &= \boldsymbol{S}(y,x)x + \boldsymbol{F}(y,x,u). \end{aligned}$$

To be able to compare the two observers, their initial values must be identical. These initial values are first chosen for the Stamnes Observer, and

[1] http://daim.idi.ntnu.no/

then used to calculate the corresponding values for the Wondergem Observer, where $\hat{\eta}_0 = \hat{y}_0$ and $\hat{\dot{\eta}}_0 = \boldsymbol{L}(y)\hat{x}_0$, and where $\hat{x}_0 = \xi_0 + \boldsymbol{K}_x(\hat{\sigma}_0, \hat{y}_0)y_0$ as defined in Chapter 4.1. To be able to compare the two observers after the simulations, the values from the ship model and the Stamnes Observer are transformed to η, velocity in NED. When evaluating the plots, different scales are used to clearly illustrate the behaviour for each case.

The initial values are chosen so that the two observers have a velocity and position that differs from the real values. Thus, the convergence time can be evaluated and compared for the two observers. Also, this is more realistic than having the correct initial values, because in real life the initial values rarely will be perfectly known in advance. However, it is important to notice that the convergence time is partly a product of tuning, and may be influenced by a change of parameters. The tuning shown below is chosen to give a compromise between short convergence time, avoiding large overshoot in both velocity and position, and achieve a low run time.

$$
\begin{aligned}
L_1 &= \begin{bmatrix} 10 & 0 & 0 \\ 0 & 10 & 0 \\ 0 & 0 & 10 \end{bmatrix} \\
L_2 &= \begin{bmatrix} 40 & 0 & 0 \\ 0 & 40 & 0 \\ 0 & 0 & 40 \end{bmatrix} \\
\bar{k}_x &= \bar{k}_y = \bar{k}_\sigma = 0.1 \\
c_f &= 1.7 \\
c_r &= 0.1 \\
\epsilon_y &= \epsilon_\sigma = \epsilon = 0.01
\end{aligned}
$$

5.1 Comparing Convergence and Run Time

In this section, different cases are chosen in order to compare the convergence properties of the two observers. Also, the run time for the different cases are to be compared. A simulation time of 3.5 seconds is chosen to

show the convergence towards the true values. The cases to be presented are:

- Case 1: Initial Values Close to the Real Values
- Case 2: Largely Deviating Initial Values
- Case 3: Noise on Measurement Signal
- Case 4: Bias in Observer Ship Model

5.1.1 Run Time

Case:	S[s]	S & W[s]	S & St[s]	S, St & W[s]
1	0.08s	0.31s	41.51s	39.20s
2	0.08s	0.37s	115.41s	115.88s
3	0.08s	8.38s	11.81min	13.71min
4	0.08s	0.31s	42.97s	40.26s

Table 5.1: The runtime of both observers when simulating over 3.5s. S = the Ship model, W = the Wondergem Observer and St = the Stamnes Observer

The execution time of both observers are shown in Table 5.1. However, the run time is not fixed for a simulation, but varies slightly for each simulation run for each case. This is causing some inconsistencies of the run times, where one would expect the sum of the run times of the individual observer simulations to be greater than the run time of the combined simulation.

Table 5.1 shows that the execution of the Stamnes Observer is significantly more time consuming than of the Wondergem Observer. The former executes even slower when the initial values for the observers deviate considerably from the ship's real initial values. When including measurement noise in the simulation, the run time also increases considerably. This is not necessarily a problem, but in order to use the observer in a real time control system, it is crucial that it can calculate the estimates in real time. The run time of the Wondergem Observer is more robust to measurement

noise, but also shows some increase. This observation can indicate that the Stamnes Observer is more difficult to implement in a realtime control system for this ship model.

Although the Stamnes Observer has an increase in runtime for both the case with noise and the case with a large error in initial values, introducing a bias in the system matrices has no impact on the run time. This is due to the fact that the observers do not have to compensate for any high frequency signal, such as when considering the case with measurement noise.

The main cause of the long simulation run time for the Stamnes Observer is very large derivatives. As the simulation uses dynamical time steps, this will lead to very small time steps, in order to return accurate results. However, an issue with the implementation of the measurement noise that may affect the run time in a negative matter, is that when the time step is reduced, the noise signal still varies with the same amplitude, and gives a new value in each time step. In effect, this causes the noise to have a higher frequency as the time step is reduced, causing further need for reduction of the time step. This can be countered by using a more sophisticated noise generator, including a filter to limit the noise frequency according to the desired sample frequency. In real life, a fixed step size will be used for the measurements, which prevents this behaviour. However, implementing the system for a real ship is out of the scope of this thesis. An alternative to avoid the very long run time for the Stamnes Observer may be to filter the position measurements before they are used in the Stamnes Observer.

5.1.2 Case 1: Initial Values Close to the Real Values

This case is chosen to investigate how the observer reacts under ideal conditions with initial values close to the real values. The initial values chosen in this case are given in Table 5.2. They are chosen to be realistic guesses, with reasonable errors from the real values. To be able to compare the initial values for both the Stamnes and the Wondergem Observer, the corresponding initial ship velocity, $\eta_0 = \begin{bmatrix} 0.1059 & 0.0890 & 0 \end{bmatrix}^T$ and initial $\hat{x}_0 = \begin{bmatrix} 0.7 & 0.7 & 0.1 \end{bmatrix}^T$ are calculated. The error, $x_0 - \hat{x}_0 =$

Initial Values	
y_0	$\begin{bmatrix} 1 & 1 & 0.5 \end{bmatrix}^T$
x_0	$\begin{bmatrix} 0.5 & 0.5 & 0 \end{bmatrix}^T$
$\hat{y}_0$	$\begin{bmatrix} 0.5 & 1.5 & 0.6 \end{bmatrix}^T$
ξ_0	$\begin{bmatrix} -16.1336 & -13.1479 & -2.4200 \end{bmatrix}^T$
r_0	0.5
$\hat{\sigma}_0$	0
$\hat{\eta}_0$	$\begin{bmatrix} 0.5 & 1.5 & 0.6 \end{bmatrix}^T$
$\hat{\dot{\eta}}_0$	$\begin{bmatrix} 0.1492 & 0.1230 & 0.0605 \end{bmatrix}^T$

Table 5.2: Initial Values, normal deviating from the ships values

$\begin{bmatrix} -0.2 & -0.2 & -0.1 \end{bmatrix}$, shows a small difference.

To get a reasonable picture of what the initial values will be in real life, the Froude scaling is used to transform the simulated values into the corresponding real size values. The velocity of a ship is usually given in knots, and is therefore presented in both knots and m/s in Table 5.3 scaled for a real size ship. As seen in Table 5.3, the initial velocity for the observers differs by approximately one knot, which is a reasonable assumption considering a real size supply vessel. The difference in position is 0.5 m in both x and y direction and 0.1 rad in yaw. This corresponds to less than half the ship length. By the Froude scaling, the distance in real life would be 40 m, which is a quite good guess.

When considering Figure 5.1 and 5.2 of the estimate error in position and velocity, respectively, the behaviour is shown to be different for the two observers. The Stamnes Observer allows a slow convergence in position in order to quickly reach the correct velocity. The Wondergem Observer, on the other hand, alter the velocity, creating a large overshoot to quickly reach the real position of the ship. Even though this behaviour is different,

Real size ship velocity	Observer velocity
2.25knot	3.15knot
1.16m/s	1.62m/s

Table 5.3: Initial velocity scaled in real size, in knot and m/s

both observers converge within two seconds for both the position and velocity estimates.

When considering Figure 5.1 of the observer position error, it is clear that the Stamnes Observer has a more damped behaviour and converges to a neighbourhood around the true position more slowly than the Wondergem Observer. The Wondergem Observer has an overshoot of 0.15 rad in yaw, but converges in about a second. Froude scaling to real size, a second corresponds to 8.37 seconds for a ship of real size. Since the observer in real life would have enough time to initialize within reasonable matters, a convergence time of 8.37 seconds would be considered acceptable.

The observer velocity error in Figure 5.2 shows similar behaviour as the position error. However, the Wondergem Observer gets a significantly larger overshoot in North, East and yaw. Also, the convergence time for both observers is very similar. The Stamnes Observer quickly finds the real velocity, and converges with a damped behaviour. The Wondergem Observer shows a slightly underdamped behaviour with a large overshoot before it converges towards the real velocity. Both observers show stability and converges towards a neighbourhood around the true value within 2 seconds, which is a reasonable result.

In real life, a short convergence time is not of a great matter, because the observer will have enough time to initialise before it will be used for control purposes. However, the fact that both observers converge within a reasonable amount of time, indicates stability of the observers.

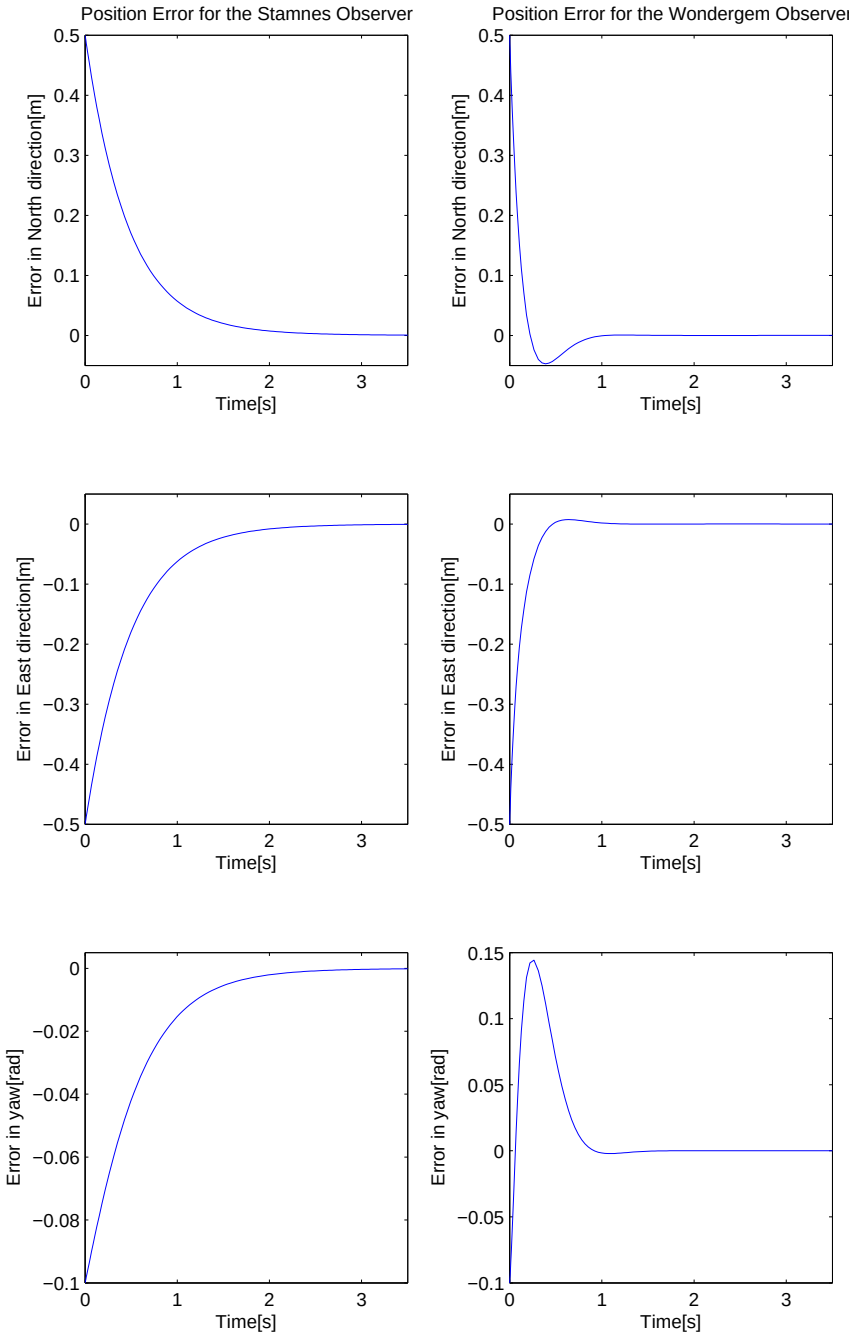

Figure 5.1: Case 1: Observer position estimate error

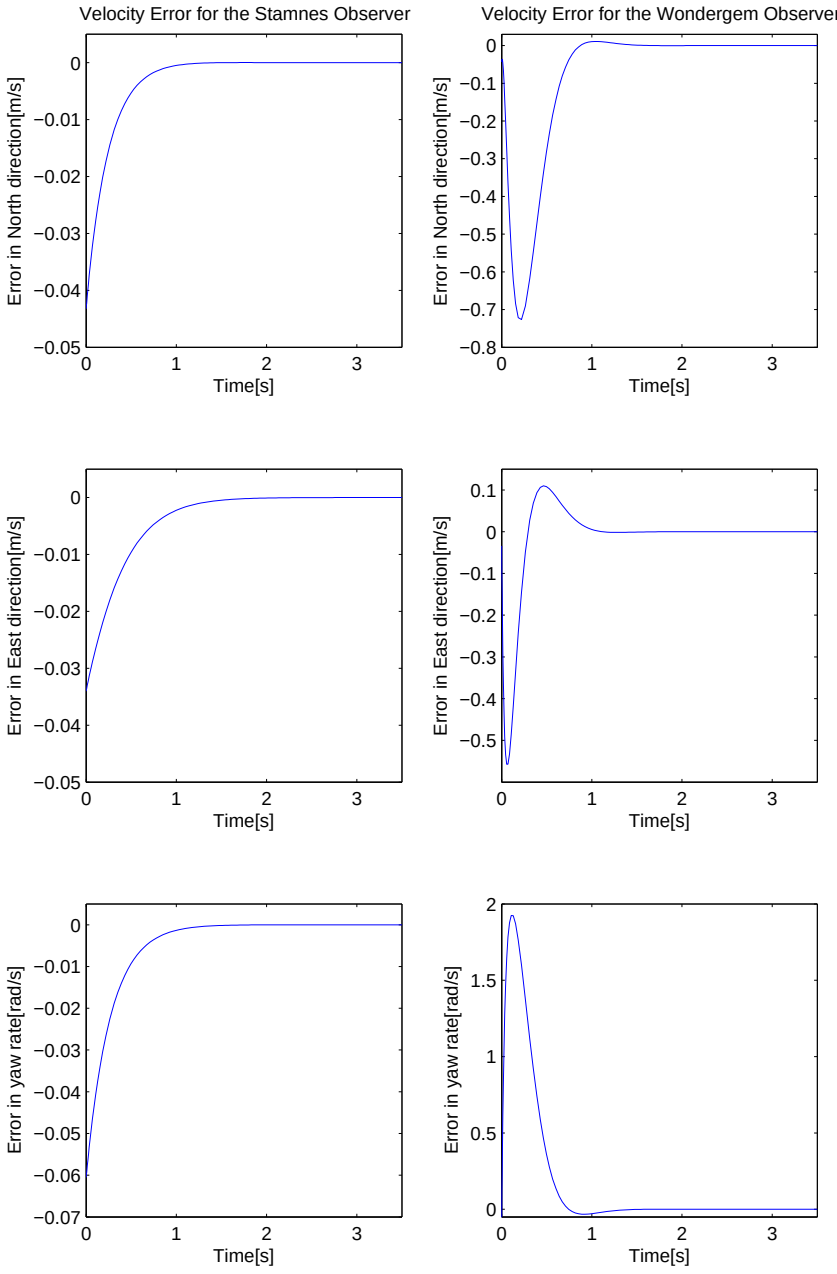

Figure 5.2: Case 1: Observer velocity estimate error

5.1.3 Case 2: Largely Deviating Initial Values

The case of largely deviating initial values is chosen to investigate how the observers are handling a yaw error of 180 degrees, and errors in North and East of approximately one boat length. A possibility is that the observers misinterpret the yaw angle, causing the observer ship to run backwards.

Initial Values	
y_0	$\begin{bmatrix} 1 & 1 & 0.5 \end{bmatrix}^T$
x_0	$\begin{bmatrix} 0.5 & 0.5 & 0 \end{bmatrix}^T$
$\hat{y}_0$	$\begin{bmatrix} 0 & 2 & 3.6416 \end{bmatrix}^T$
ξ_0	$\begin{bmatrix} -14 & -13.5 & -2 \end{bmatrix}^T$
r_0	0.5
$\hat{\sigma}_0$	0
$\hat{\eta}_0$	$\begin{bmatrix} 0 & 2 & 3.6416 \end{bmatrix}^T$
$\hat{\dot{\eta}}_0$	$\begin{bmatrix} 0.3700 & 0.3080 & 0.2767 \end{bmatrix}^T$

Table 5.4: Initial values, deviating largely from real values

As previously mentioned, both observers have equivalent initial conditions. The corresponding initial ship velocity, $\eta_0 = \begin{bmatrix} 0.1059 & 0.0890 & 0 \end{bmatrix}^T$, and the initial $\hat{x}_0 = \begin{bmatrix} 1.7225 & 1.7711 & 0.4572 \end{bmatrix}^T$ is found to be able to compare the initial conditions to the ship and the observers. The ship velocity differs from the observer initial velocity, as seen from Table 5.5, by 5.58 knots. A difference of this size can be considered a large difference as the maximum speed of a supply vessel normally is around 15-17 knots.

When considering the position error plots for the two observers in Figure 5.3, the first thing to notice is that the convergence time is similar as for Case 1, for the Wondergem Observer. For the Stamnes Observer, the convergence time reduces. This is because the Stamnes Observer has

Real size ship velocity	Observer velocity
2.25knots	7.83knots
1.16m/s	4,03m/s

Table 5.5: Initial velocity converted to real ship in knots and m/s

dynamic gains which increase when the difference is large, causing the convergence to be more rapid. At the same time, the Wondergem Observer responds with a larger overshoot in x, North direction, and yaw. Both observers manage to find the correct yaw angle.

The observers have a quite similar behaviour in velocity estimation error as in position estimation error. As seen in figure 5.4, the convergence time for the Stamnes Observer behaves in a similar manner in Case 1 and Case 2. The Wondergem Observer has, as for the position estimation error, a larger overshoot than for Case 1, but finds the real position within 1.5 seconds, which is an acceptable result. Both observers show a stable result by converging towards zero error within a short amount of time, which is the desired behaviour.

To conclude, the Stamnes Observer has proven to be the better observer for this case regarding convergence time, and at the same time, avoiding an overshoot.

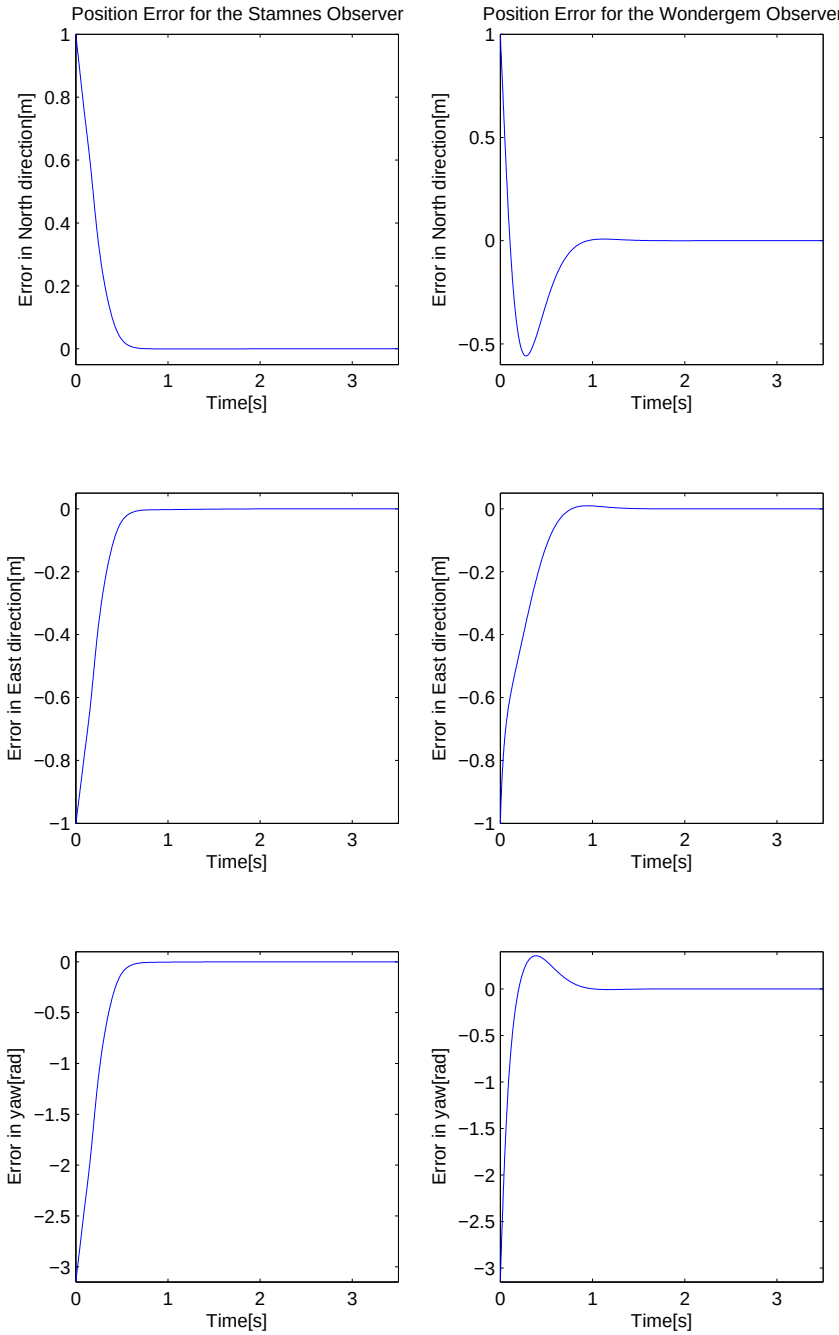

Figure 5.3: Case 2: Observer position estimate error

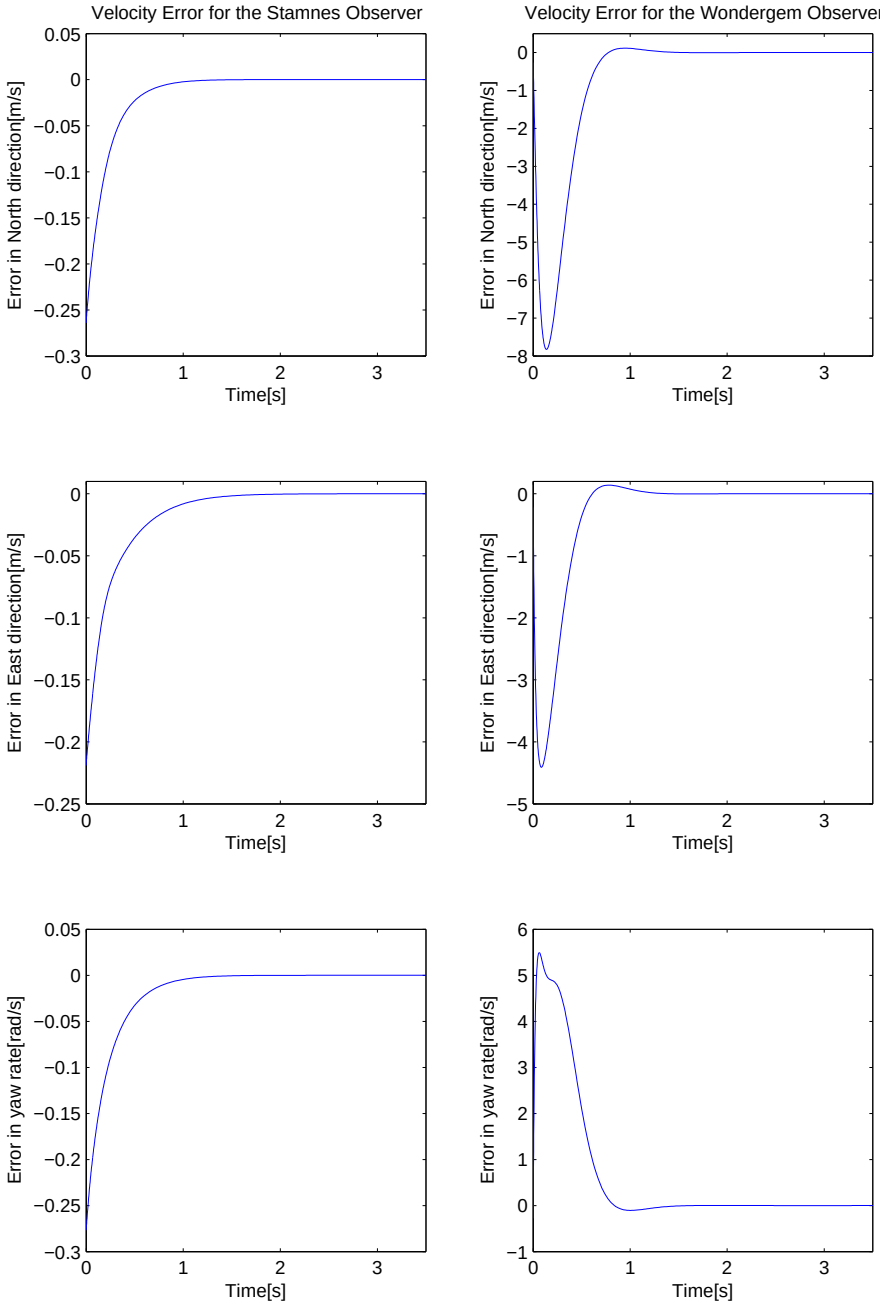

Figure 5.4: Case 2: Observer velocity estimate error

5.1.4 Case 3: Noise on Measurement Signal

This case is chosen to illustrate how the convergence of the observers react to high frequency measurement noise. The noise is added to the position measurement available for the two observers. It is added as a scaled random signal simulating white noise. The initial values are the same as in Case 1.

When studying Figure 5.5 and 5.6, it is clear that the Stamnes Observer is highly affected by adding the measurement noise. The position estimation errors in North and East directions do not manage to converge within 3.5 seconds and the velocity estimation errors clearly diverge in the given directions. On the other hand, the Wondergem Observer handles the noise very well, reacting very similar to Case 1 without noise. When zooming in on the signal, it is visible that the error in both velocity and position is not completely zero, but stays in a neighbourhood around zero with a low amplitude noise. However the amplitude is so small that it can be ignored.

To reduce the influence the measurement noise has on the Stamnes Observer, increasing the tuning parameters, $\bar{k}_x$, $\bar{k}_y$ and $\bar{k}_\sigma$ is an option. As seen in Figure 5.8, by increasing $\bar{k}_x$, $\bar{k}_y$ and $\bar{k}_\sigma$, the observer becomes less noise sensitive and converges faster in velocity, but also slower in the position convergence. This can be improved by increasing the initial value of r_0 and σ_0, but then the runtime again increases, and also a small bias in the velocity becomes present. By keeping $r_0 = 0.5$, and increasing $\hat{\sigma}_0$ from 0 to 0.5, and also increasing $\bar{k}_x$, $\bar{k}_y$ and $\bar{k}_\sigma$ from 0.1 to 0.5, the observer quickly converges in velocity, but gets a slow convergence in position. This can clearly be seen in Figure 5.7 of the position estimate error and Figure 5.8 of the velocity estimate error with the new tuning. Because of the large overshoot in the Wondergem Observer, the scale is much larger. That makes the noise in the Wondergem Observer not visible, but when zooming in on the Figure 5.8, it has the same amplitude as the Stamnes Observer.

The Wondergem Observer is clearly more robust for measurement noise, even though proper tuning improves the convergence properties for the Stamnes Observer. For the former, the influence of the measurement noise is seen to be minimal.

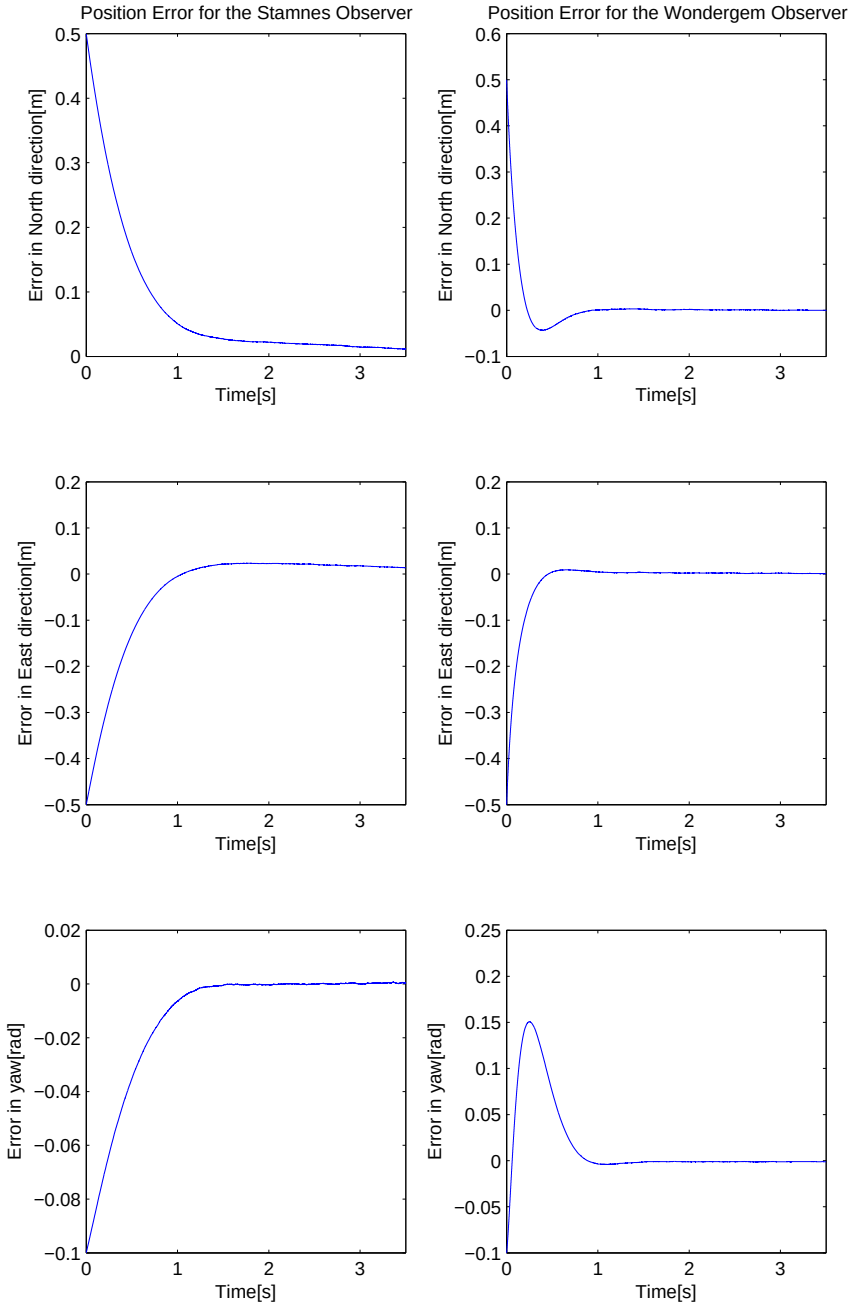

Figure 5.5: Case 3: Measurement noise, observer position estimate error

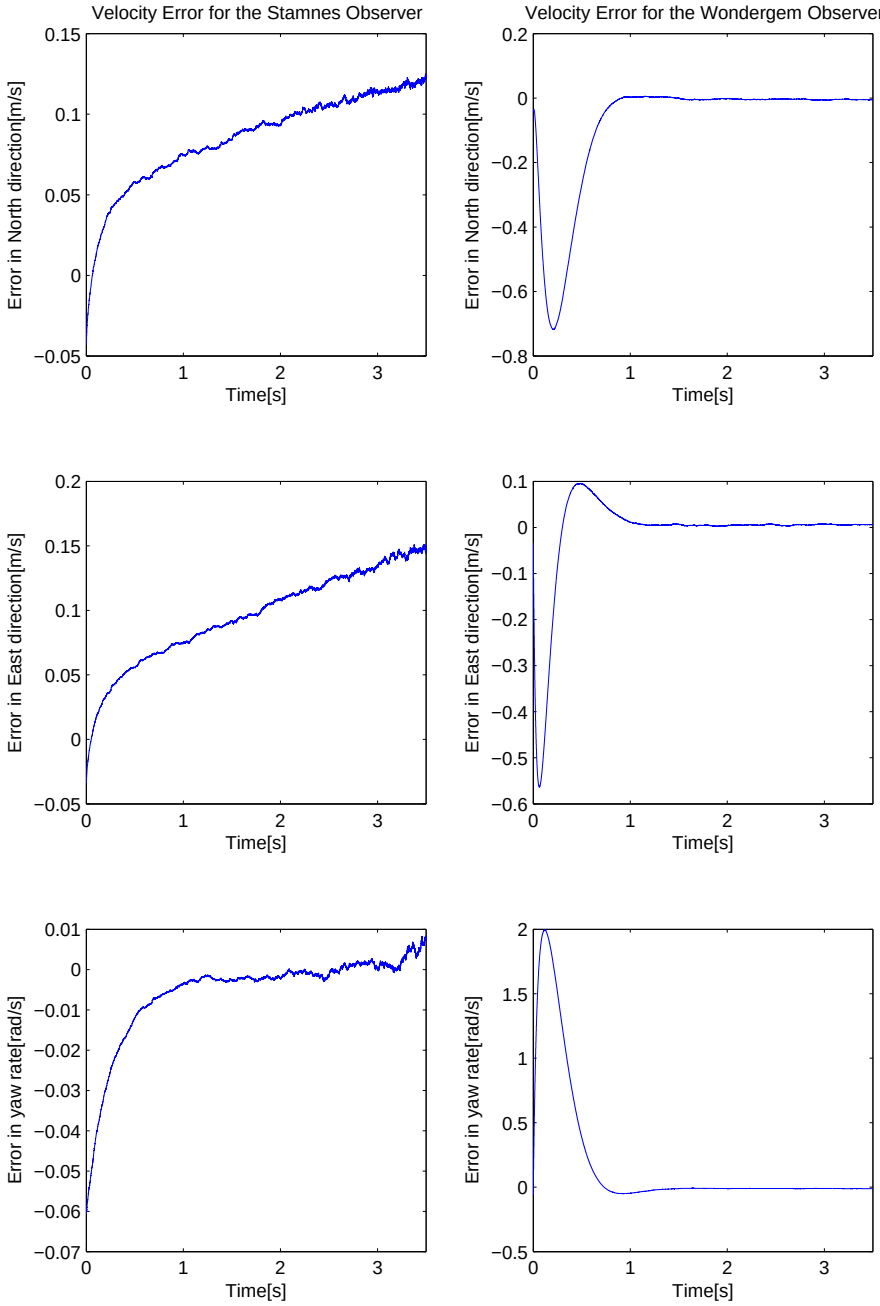

Figure 5.6: Case 3: Measurement noise, observer velocity estimate error

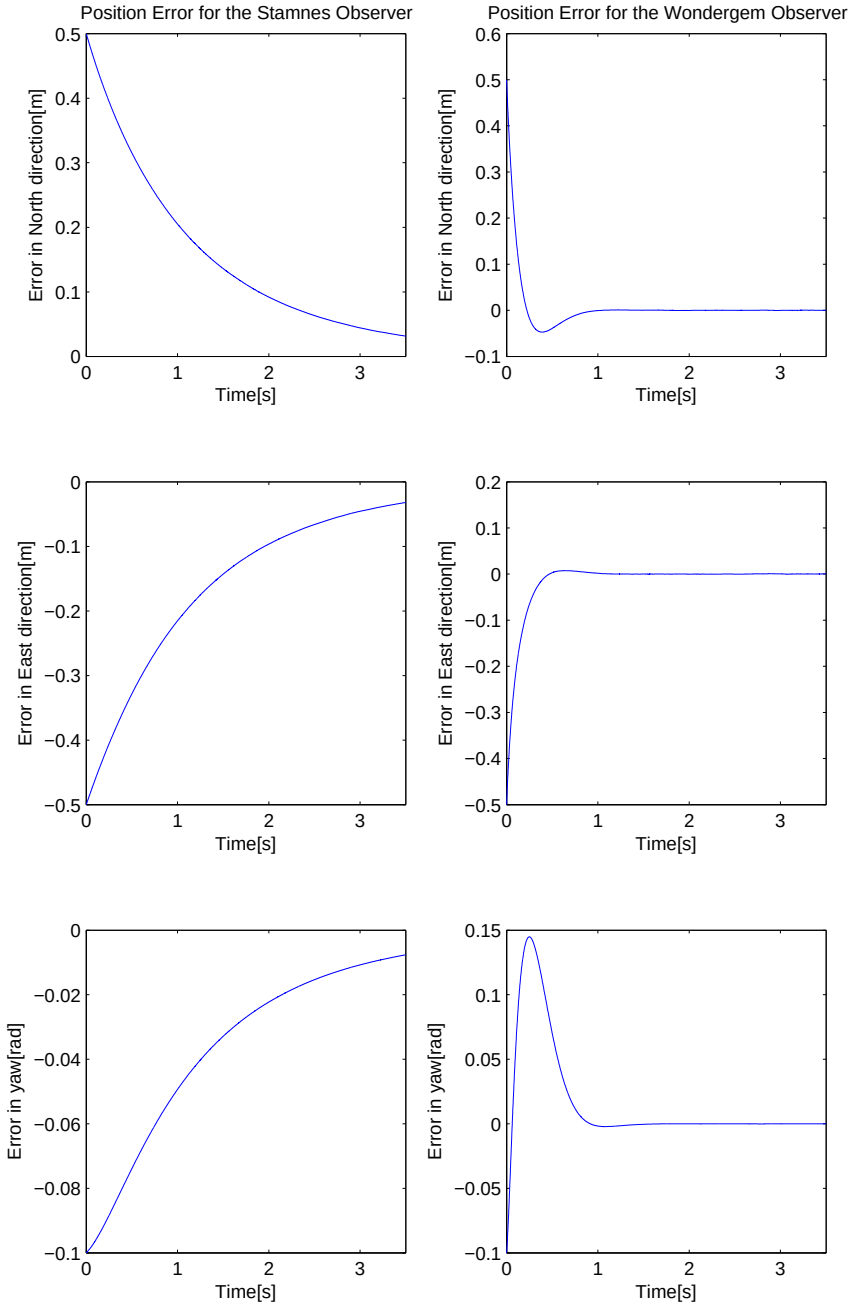

Figure 5.7: Case 3: The new tuning adapted to the system with measurement noise, observer position estimate error

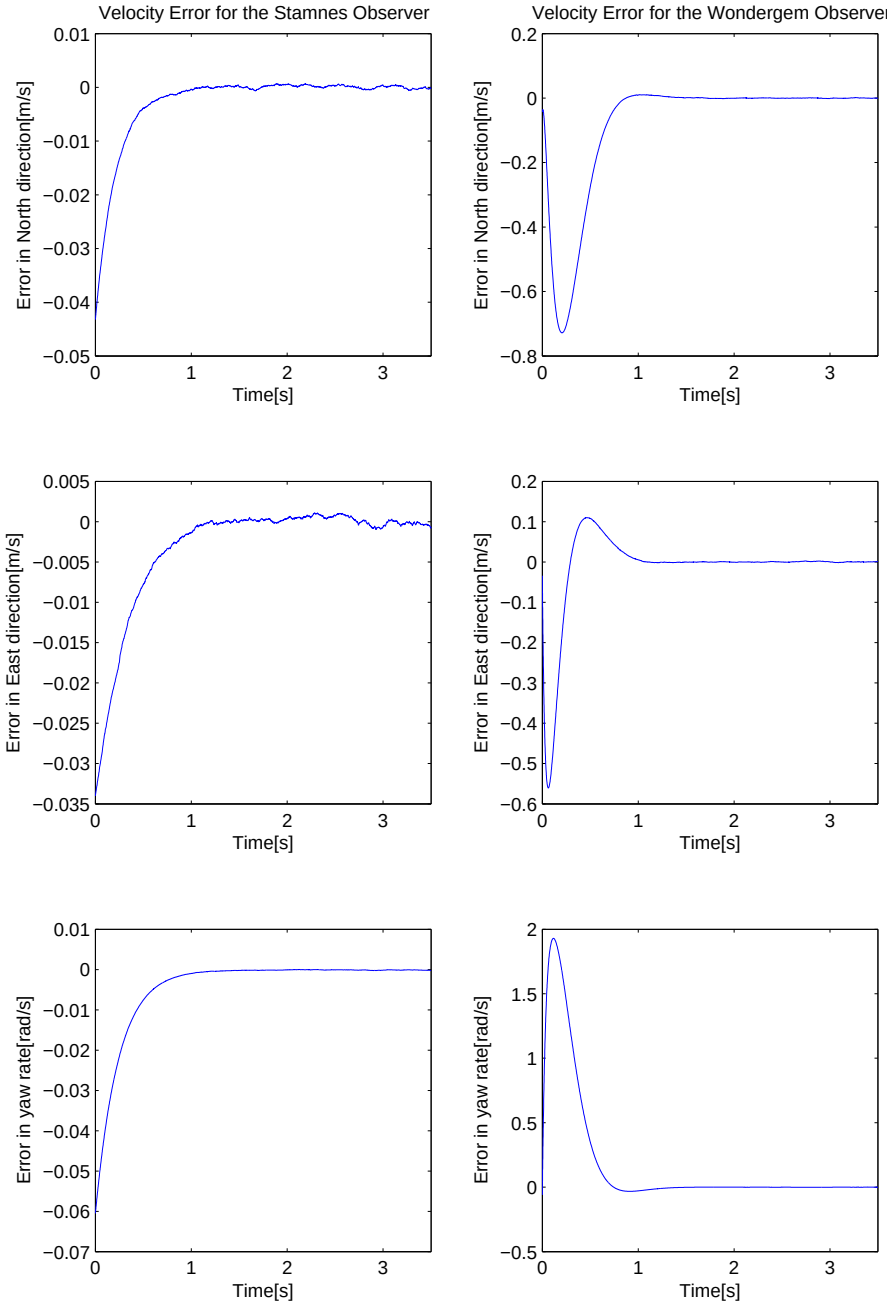

Figure 5.8: Case 3: The new tuning adapted to the system with measurement noise, observer velocity estimate error

5.1.5 Case 4: Inaccuracies in Observer Ship Model

The case with inaccuracies in the observer ship model is included to show the robustness in the observers. In a real case, the ship model attained in the observers is rarely perfect. The mass matrix and Coriolis can be found quite accurately, but the non-linear damping is extremely difficult to find accurately (Fossen [2011]). A small bias is therefore added in the damping matrix, and a bias with a very low scale is added to the mass, and the Coriolis matrix. The initial values are chosen to be the same as in Case 1.

As seen in Figure 5.9, the estimated position is not affected by the bias in the system equations. This is because of the nature of the position estimate of both observers. Since the position is measured, and the position estimation error is used as a correction term, the position is less dependent of a correct ship model for an accurate result, than for the velocity estimate.

The estimated velocities in Figure 5.10 have a small bias in North and East direction in both the Stamnes and the Wondergem Observer. Due to the large overshoot in the Wondergem Observer, the bias is barely visible, but when zooming in, it has the same amplitude as the Stamnes Observer. The bias is present because the model equations of the ship are used to calculate the velocity estimate in both the observers, causing them to have a small bias when inaccuracies in the system equations is present. This factor emphasises that both observers require an accurate model of the ship to be able to estimate the correct velocity.

The bias is, on the other hand, small and would for the largest bias of 0.003m/s in Figure 5.10 correspond to a fault of 0.025 m/s for a ship of full size. The bias is so small that it can be ignored, and a conclusion can be made that the two observers handle a bias in the system matrices very well, and converge towards a neighbourhood around the real value in a stable matter.

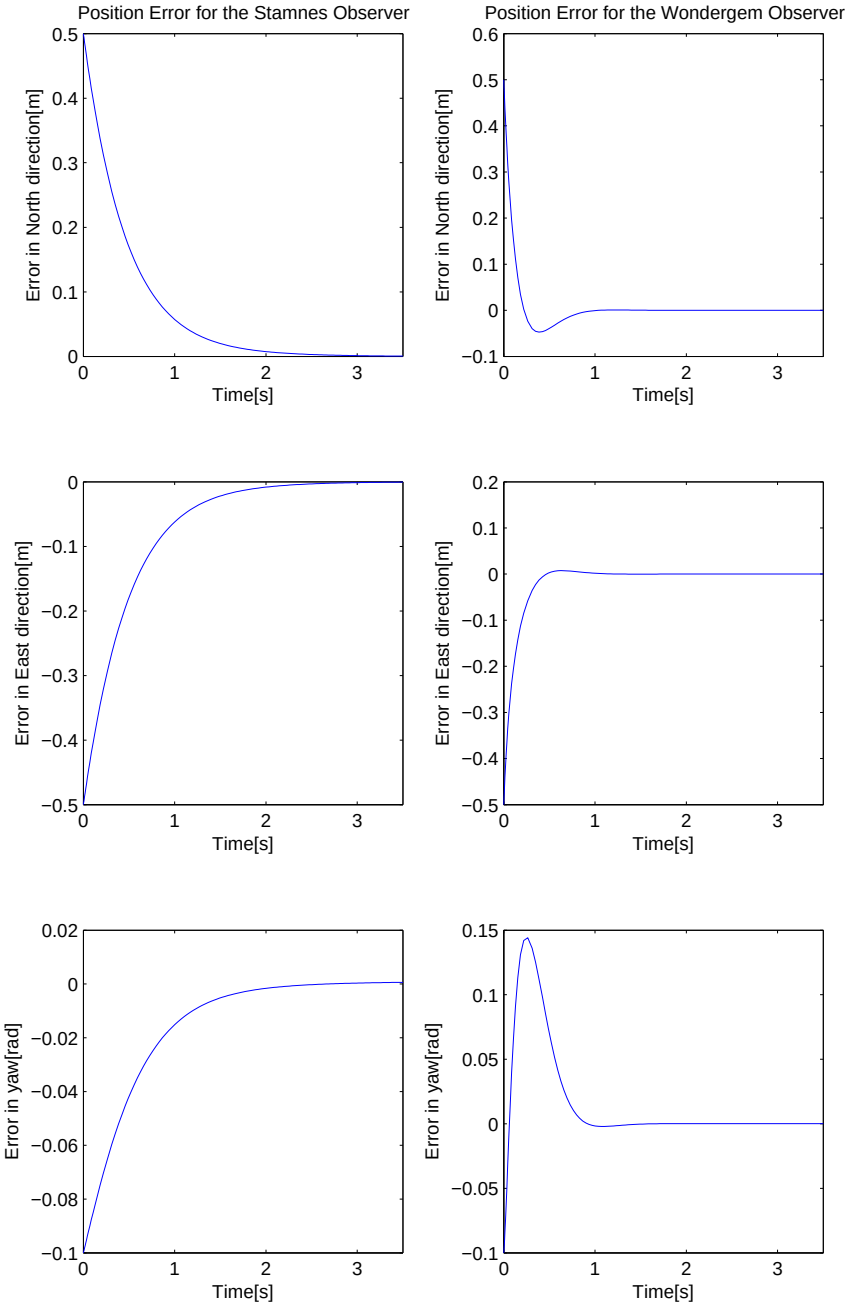

Figure 5.9: Case 4: Bias in observer ship model, observer position estimate error

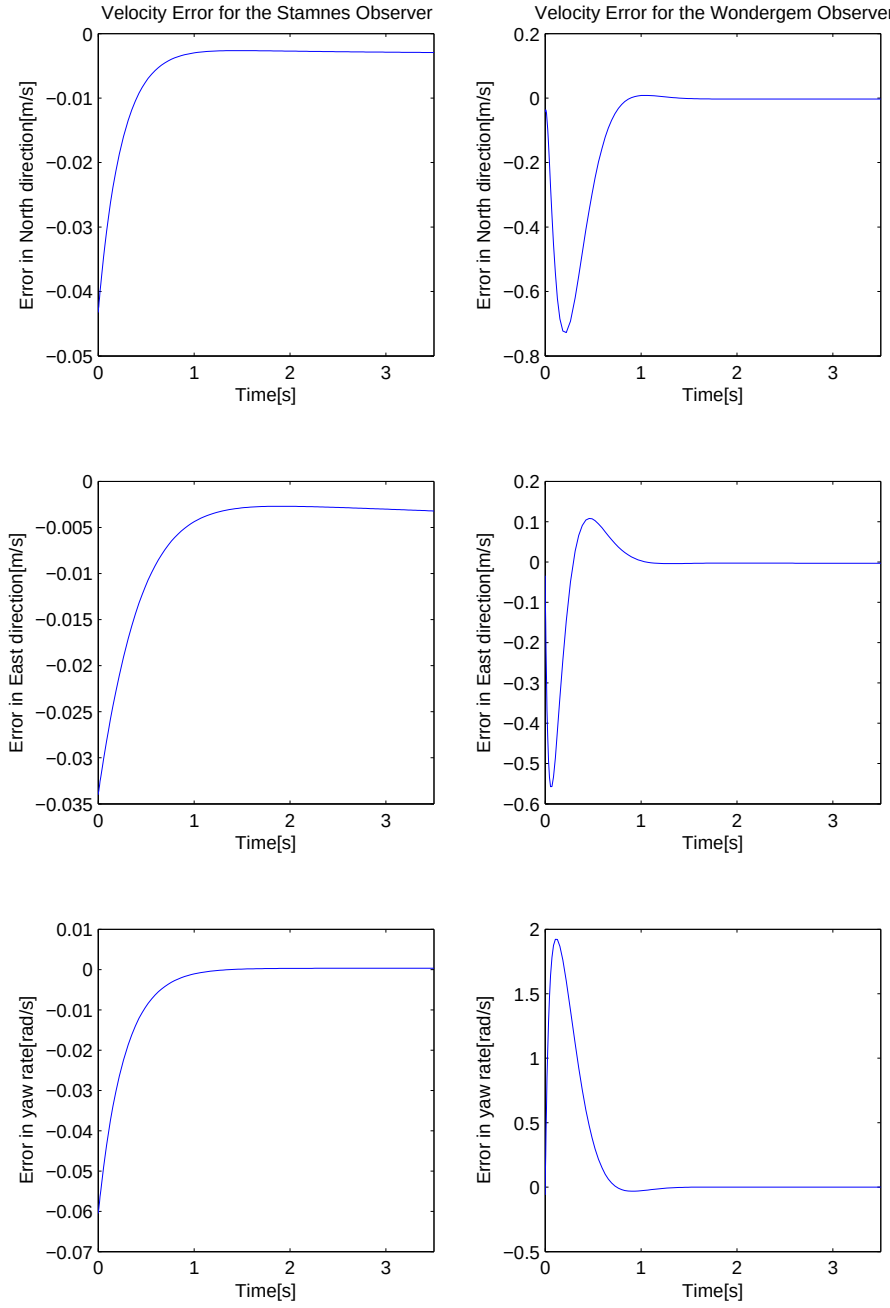

Figure 5.10: Case 4: Bias in observer ship model, observer velocity estimate error

5.2 Investigating the Stability of the Observers

This section considers the stability of the observers when simulating in 1000 s, and their behaviour when sudden excitations are made to the ship. In addition, the simulation is performed over a long timespan, to clearly show the observers' abilities to follow the real value over time.

5.2.1 Case 1: Increasing Input Stepwise

The case with the input increasing stepwise, is chosen to get "jumps" in the velocity in a short amount of time. When exciting the system in this matter, it is possible to study the stability of the observers. Additionally, the ability to follow the real value during sudden changes to the system is shown.

As seen in Figure 5.11, the velocity increases in the North direction, when the time reaches 300 seconds and again at 600 seconds. After each change in input, the estimated ship velocity oscillates before it settles. As seen in Figure 5.11, both the Stamnes Observer and the Wondergem Observer follows the ships movement perfectly. This can be explained by the observers' use of a perfect ship model, and of scaling, making the low amplitude noise not visible.

Figure 5.12 shows some oscillations in the velocity estimation error plots for the Stamnes Observer when the velocity increases. As shown in Figure 5.13 the Stamnes Observer also gets a noisy behaviour in position estimation error for the high input values. A reason for that can be the numerical operations making the results less accurate when the velocity increases. As seen in Figure 5.13 these rapid changes are also causing a bias in the position estimates, especially in the North direction. The reason for the North direction to be more affected is related to the heading of the ship.

However, these velocity estimation errors are within a small neighbourhood around zero, and can be considered insignificant.

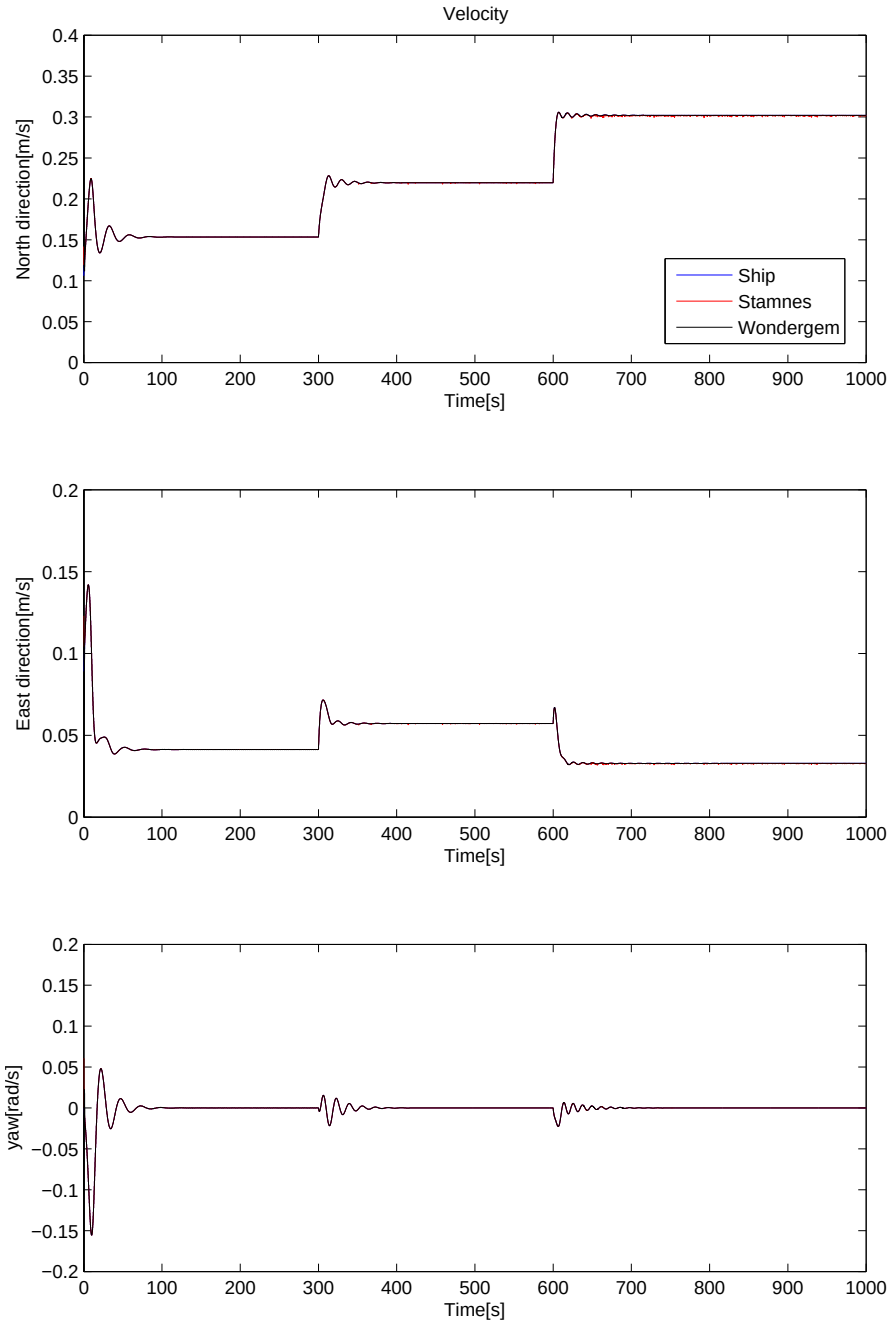

Figure 5.11: Case 1: Ship and observer velocity in NED

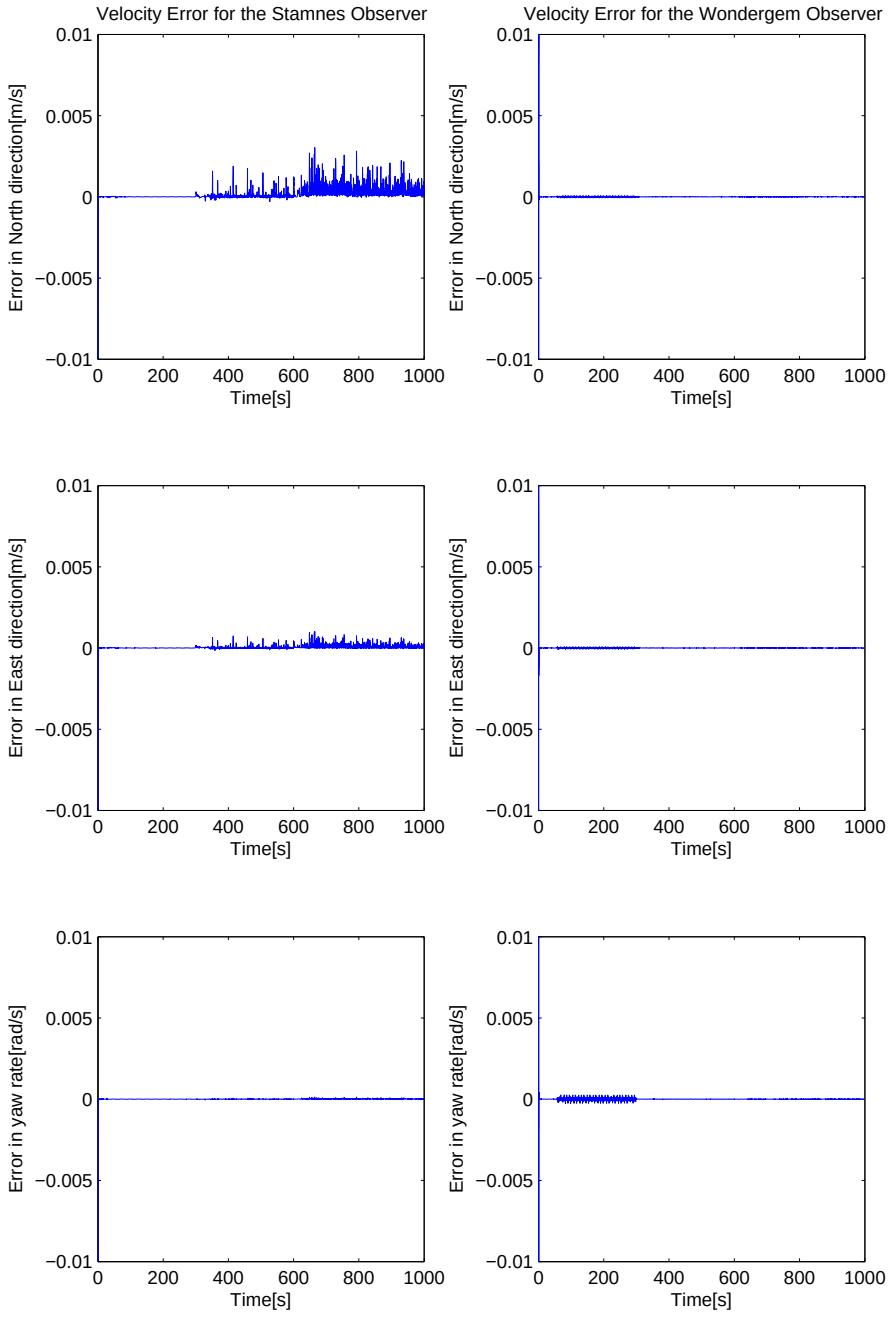

Figure 5.12: Case 1: Observer velocity estimate error

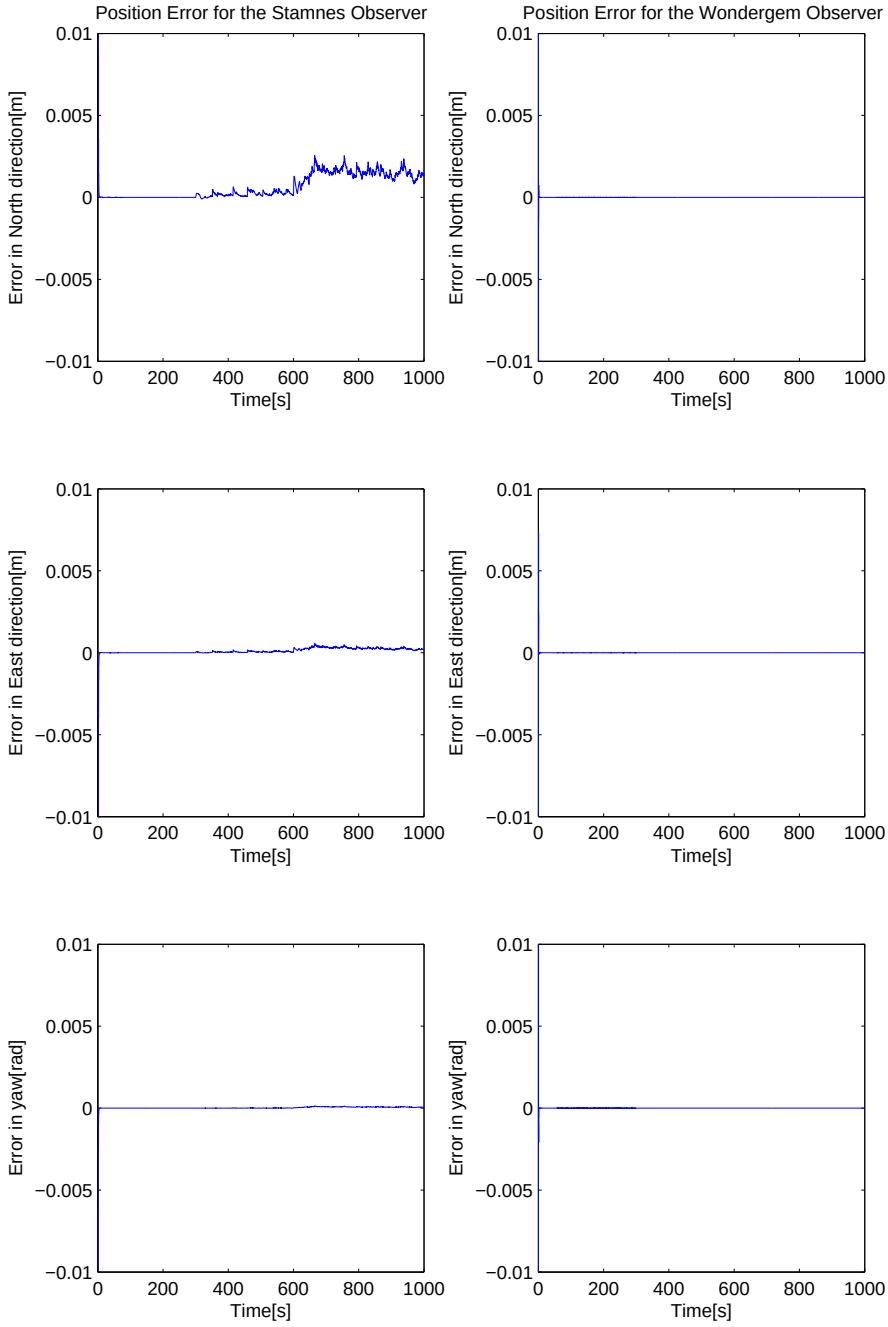

Figure 5.13: Case 1: Observer position estimate error

5.2.2 Case 2: Increasing Input Stepwise with Bias in the Observer Ship Model

When adding model bias in the observer model, the robustness of the observers is shown. Figure 5.14 shows that a constant bias is present in the estimated velocity for both observers. This is confirmed by Figure 5.15 of the velocity estimate error. The increasing noise in the velocity estimation error for the Stamnes Observer is present also in this case. Furthermore, the bias is dependent on the input of the ship, and the velocity error changes each time the input to the system changes. Both the Wondergem Observer and the Stamnes Observer react in the same manner, and even with the small bias, both stay within a neighbourhood of the true value. This is because of the imperfect system matrices of the observers, causing the ship model to react slightly different than the real ship to the change in inputs. The change in bias in the position estimation error for both observers seen in Figure 5.16 can be explained by the same reasons as the change in bias for the velocity estimation error.

Both observers react in the same way to the bias in the system equations for the observer ship model. However since the Wondergem Observer does not output noise when the input increases, this observer proves to be the better choice for this case.

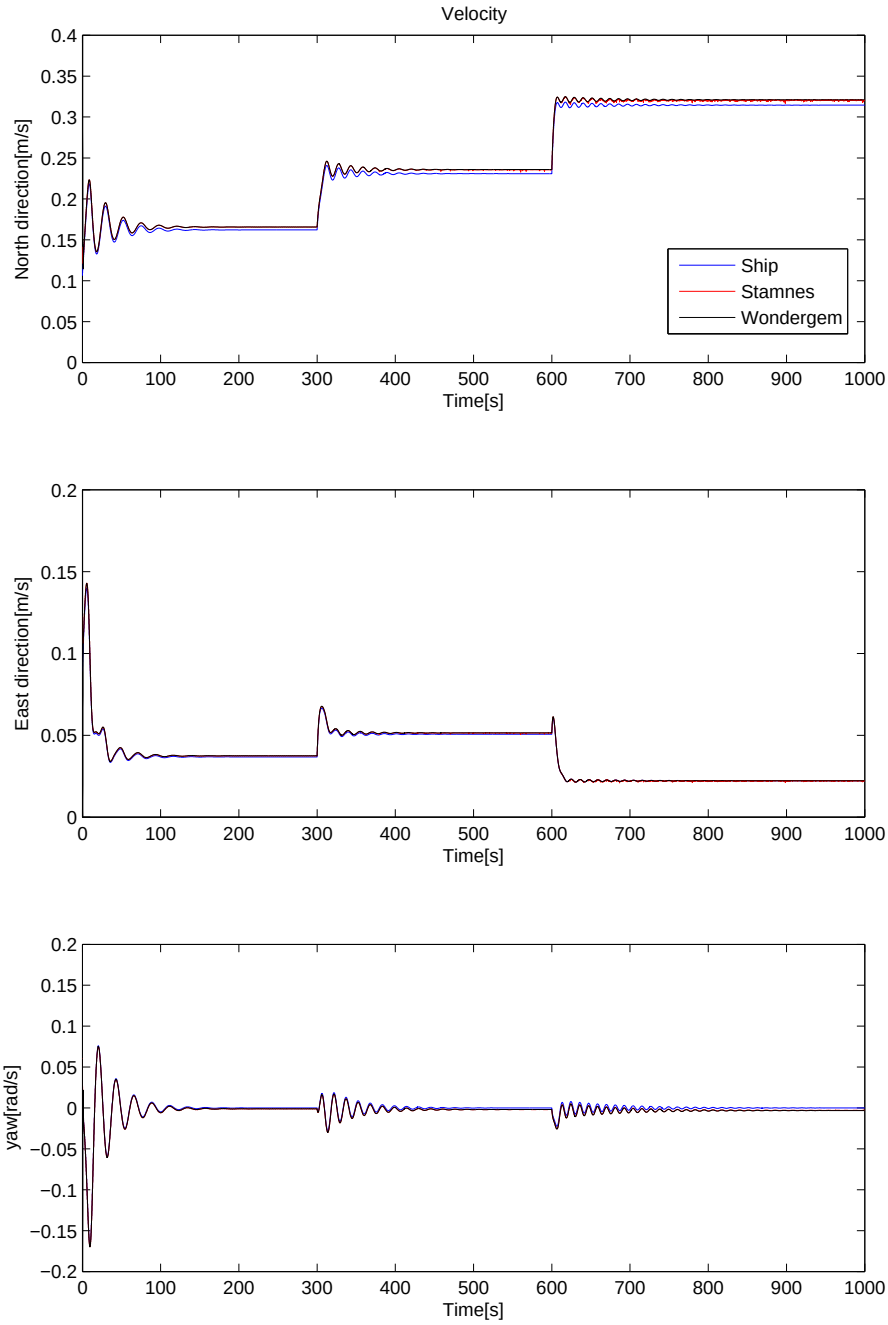

Figure 5.14: Case 2: Bias in observer ship model, ship and observer velocity in NED

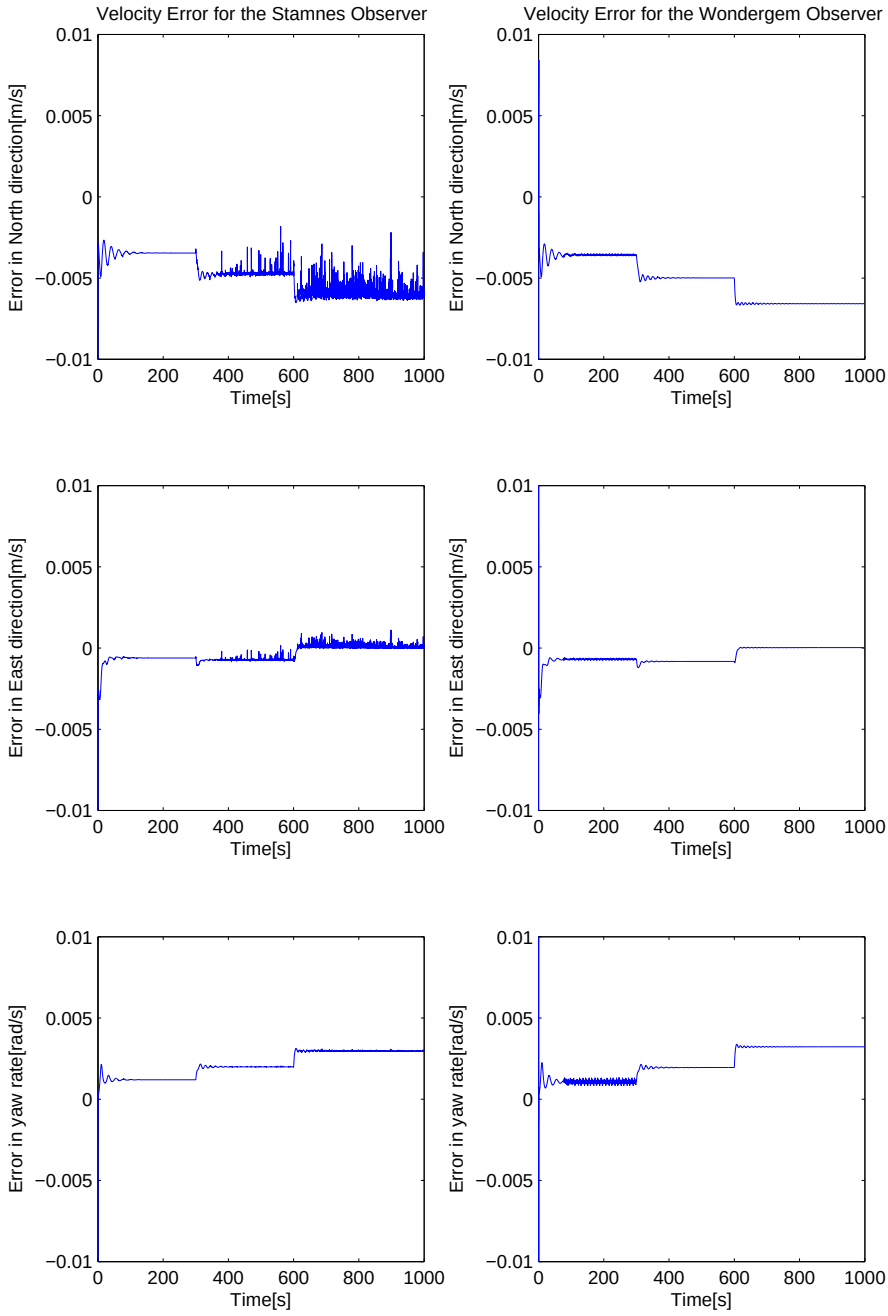

Figure 5.15: Case 2: Bias in observer ship model, observer velocity estimate error

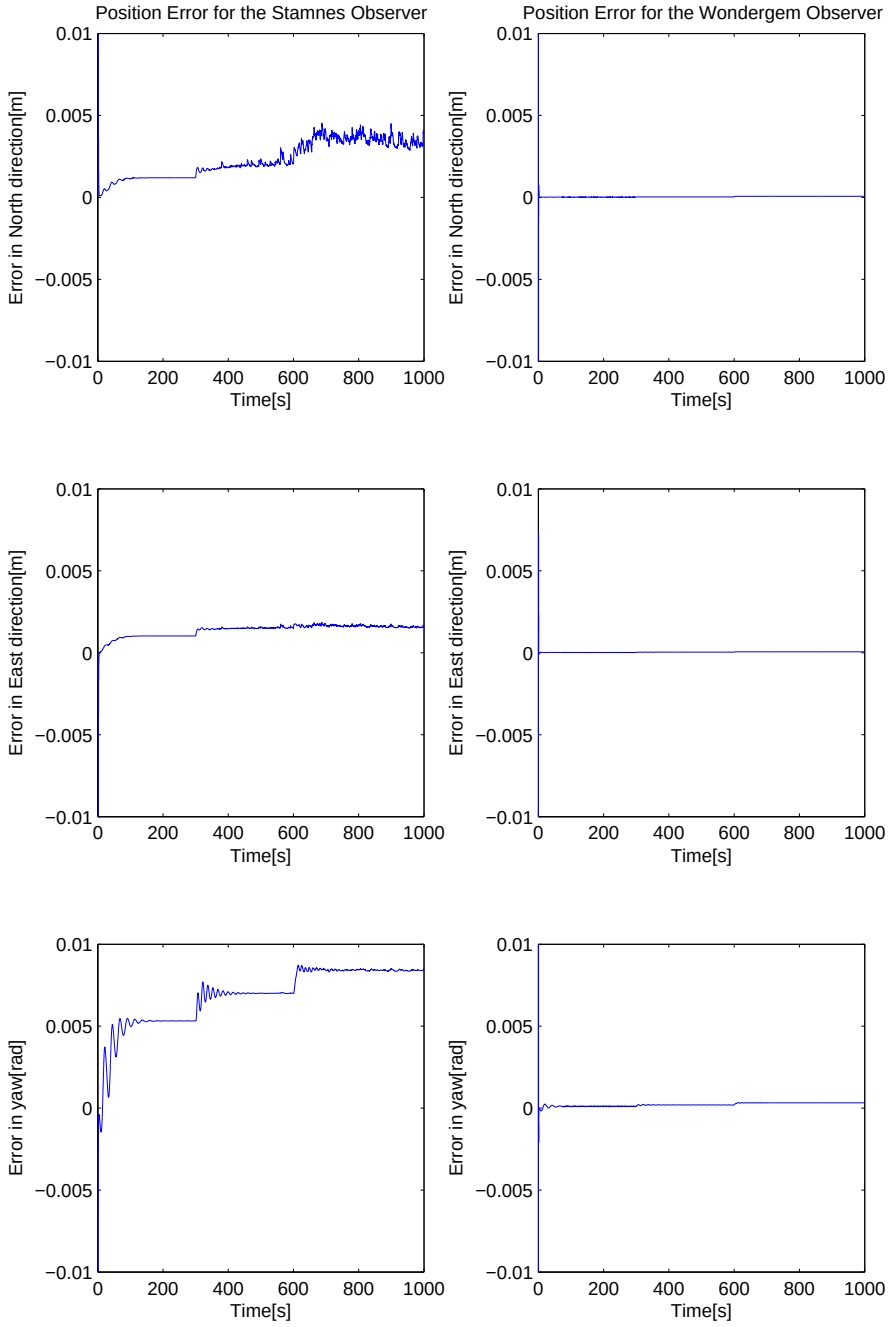

Figure 5.16: Case 2: Bias in observer ship model, observer position estimate error

5.2.3 Case 3: Increasing Input Stepwise with Measurement Noise

This case shows how the observers are handling the steps in input when measurement noise is added. However, the system with the Stamnes Observer is too computation intensive to simulate with noise for 1000 seconds, and therefore only error plots of the Wondergem observer will be shown.

As expected, the observer converges quickly and stays in a neighbourhood around the true value. The observer has no internal filtering and is influenced by the measurement noise, causing the estimated velocity to be a noisy signal. For the signal to be used in a regulator, filtering of the signal would be necessary. However, the amplitude of the noise is so small that it can be considered insignificant.

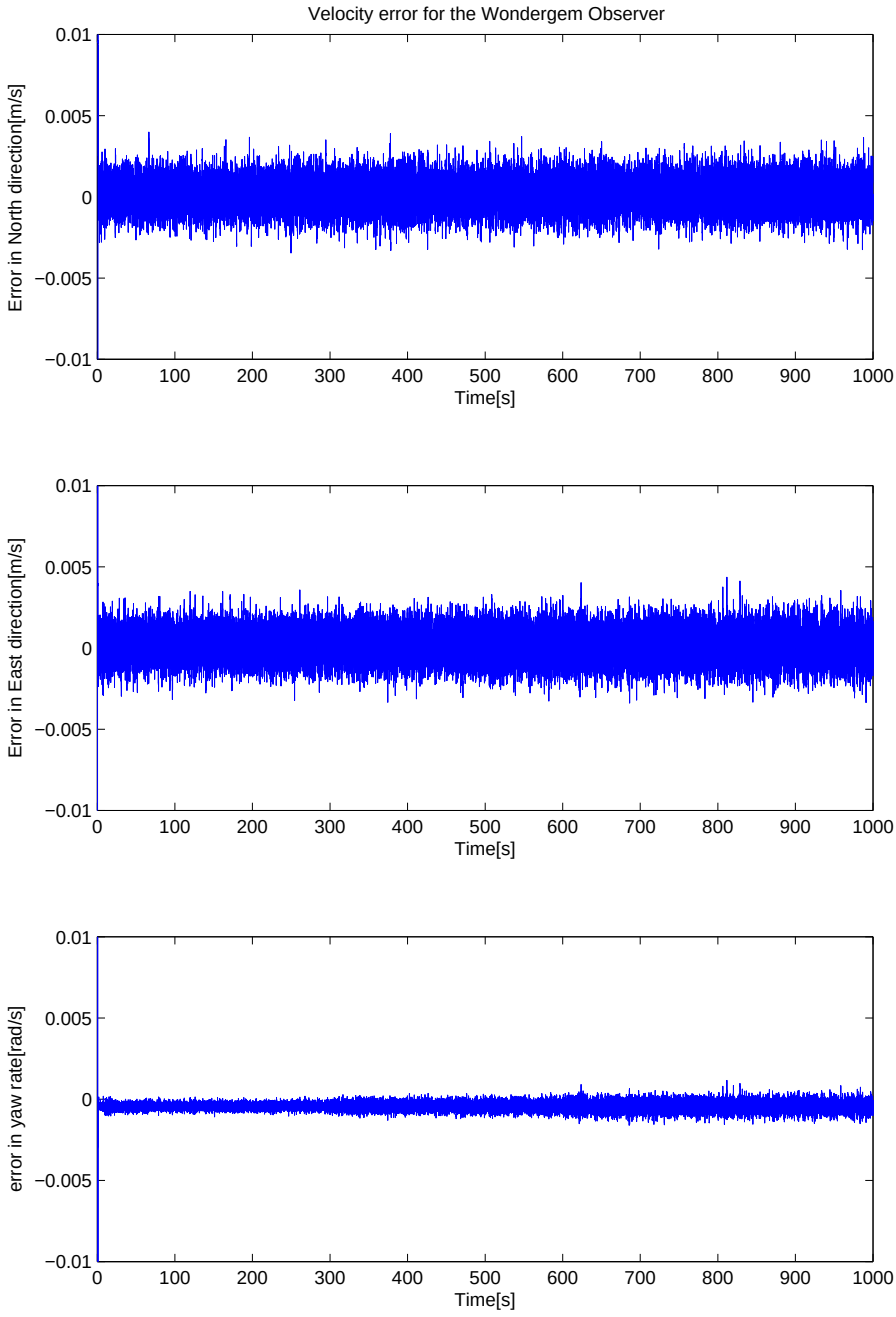

Figure 5.17: Case 3: The Wondergem Observer velocity estimate error

5.2.4 Case 4: Circular Path with Bias in the Observer Ship Model

This case is included to show how the observers react to change in direction when adding bias to the system matrices. As seen in Figure 5.18, the chosen path has an oval shape with a major axis of approximately 9.5 meters. By the use of the Froude scaling defined in Chapter 2.2, the real size diameter corresponds to 674 meters.

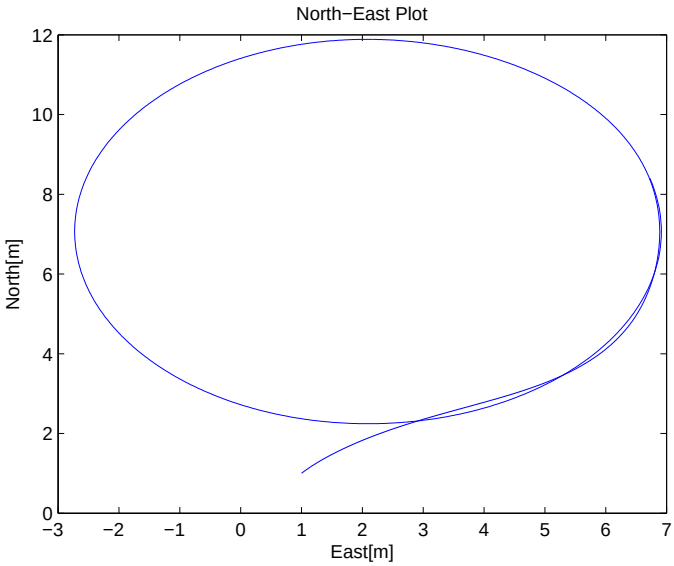

Figure 5.18: Case 4: Path of the ship

When comparing Figure 5.19 and 5.21, it is clearly seen that the estimation error in the North direction correlates to the change in velocity. This confirms the assumption in Section 5.2.2 that the bias in the velocity error is highly dependent of the velocity of the ship in a given direction. When looking on the size of the bias, it has an amplitude on 0.006 m/s which scaled to the real value corresponds to an amplitude of 0.05 m/s. A bias of this value is so small that it is not expected to affect the velocity control in a regulator.

Both observers react the same way to the velocity estimate error, but when considering the position estimate error for the two observers in Figure 5.15 the Wondergem Observer is clearly much less affected of the bias than the Stamnes Observer. This behaviour is similar to Case 2. This difference is small and can be explained by a lack of accuracy caused by the numerical elements in the simulation. However, the error is so small , that it can be considered insignificant for regulation purposes. The Wondergem Observer presents slightly better due to the better performance of the position estimate.

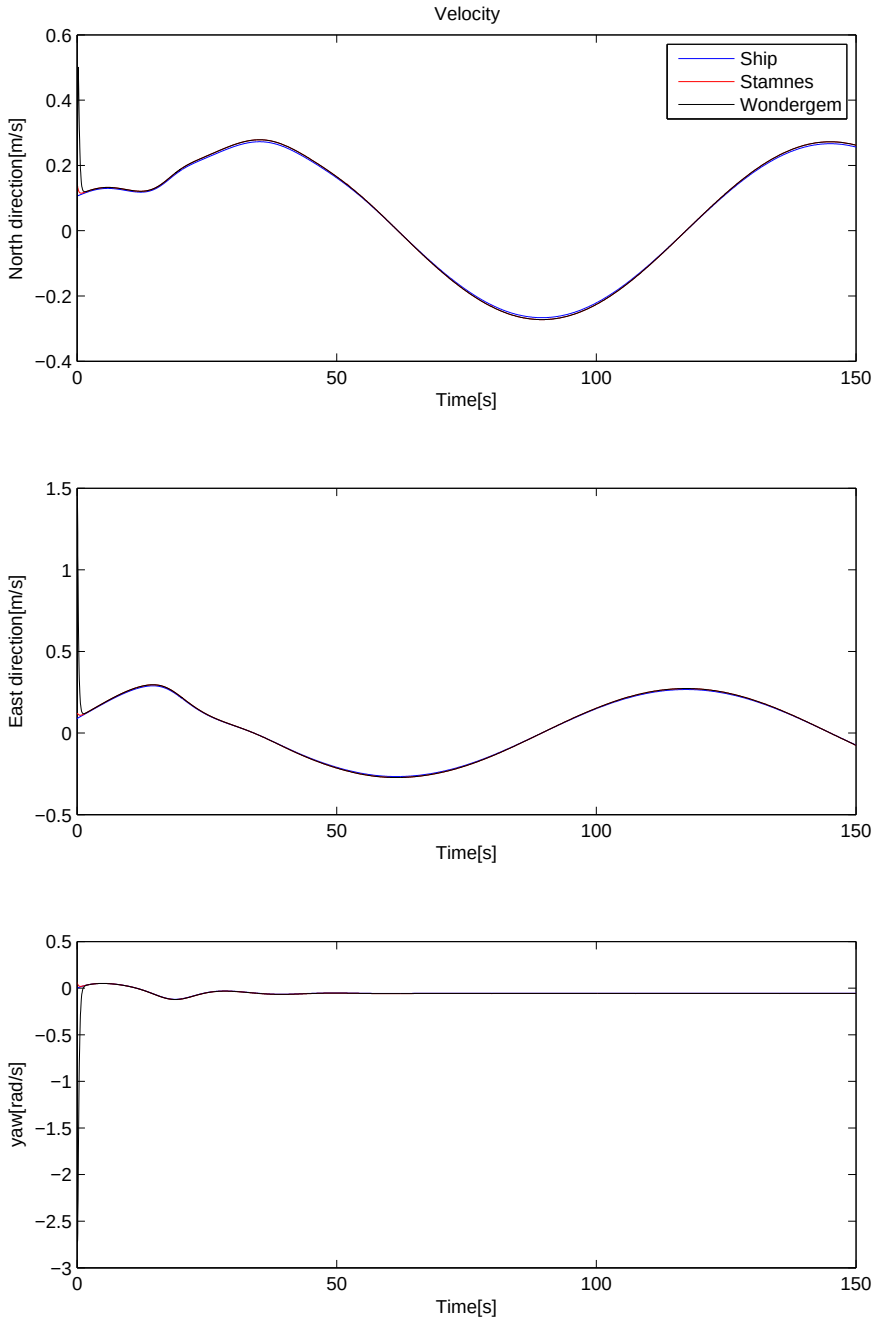

Figure 5.19: Case 4: Bias in observer ship model, circular path, ship and observer velocity in NED

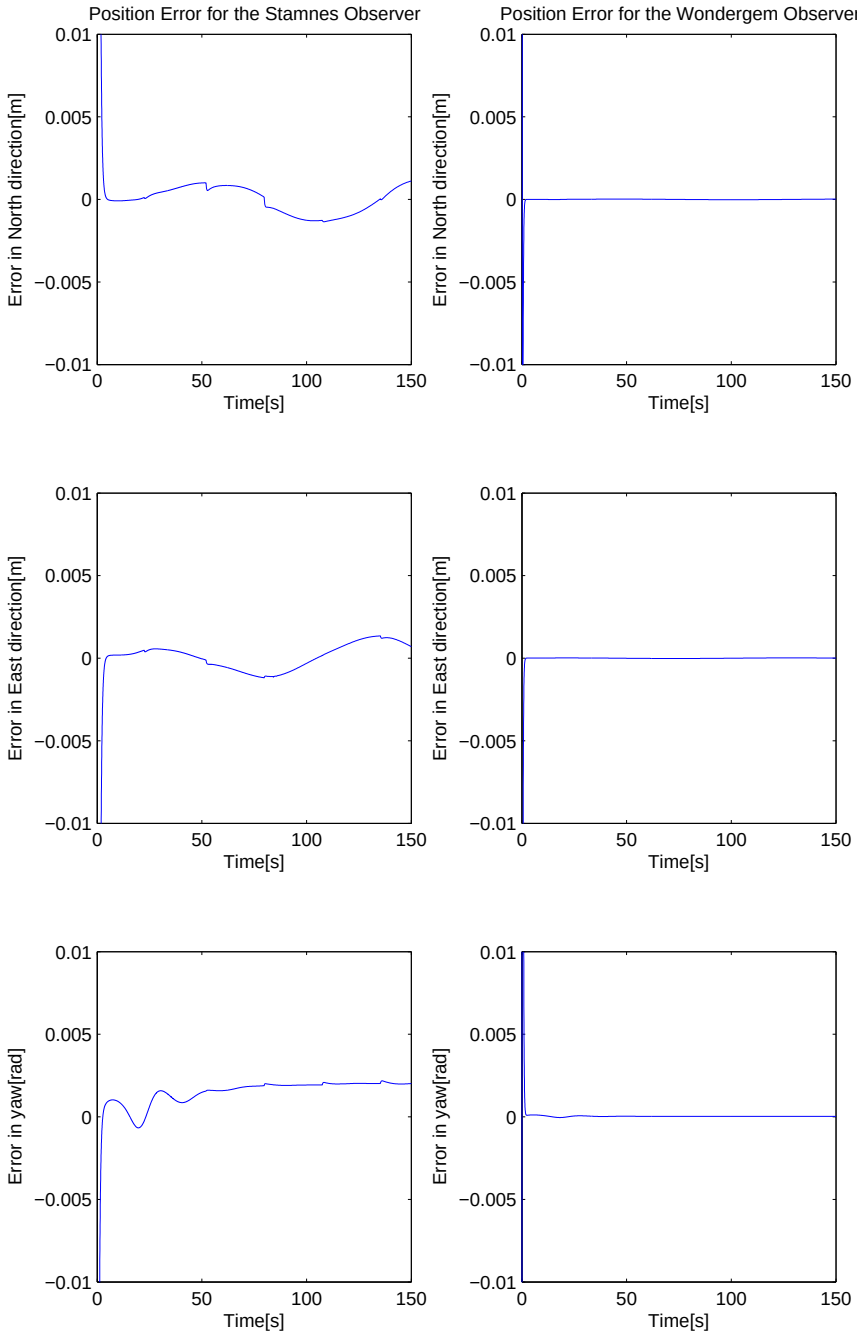

Figure 5.20: Case 4: Bias in observer ship model, circular path, observer position estimate error

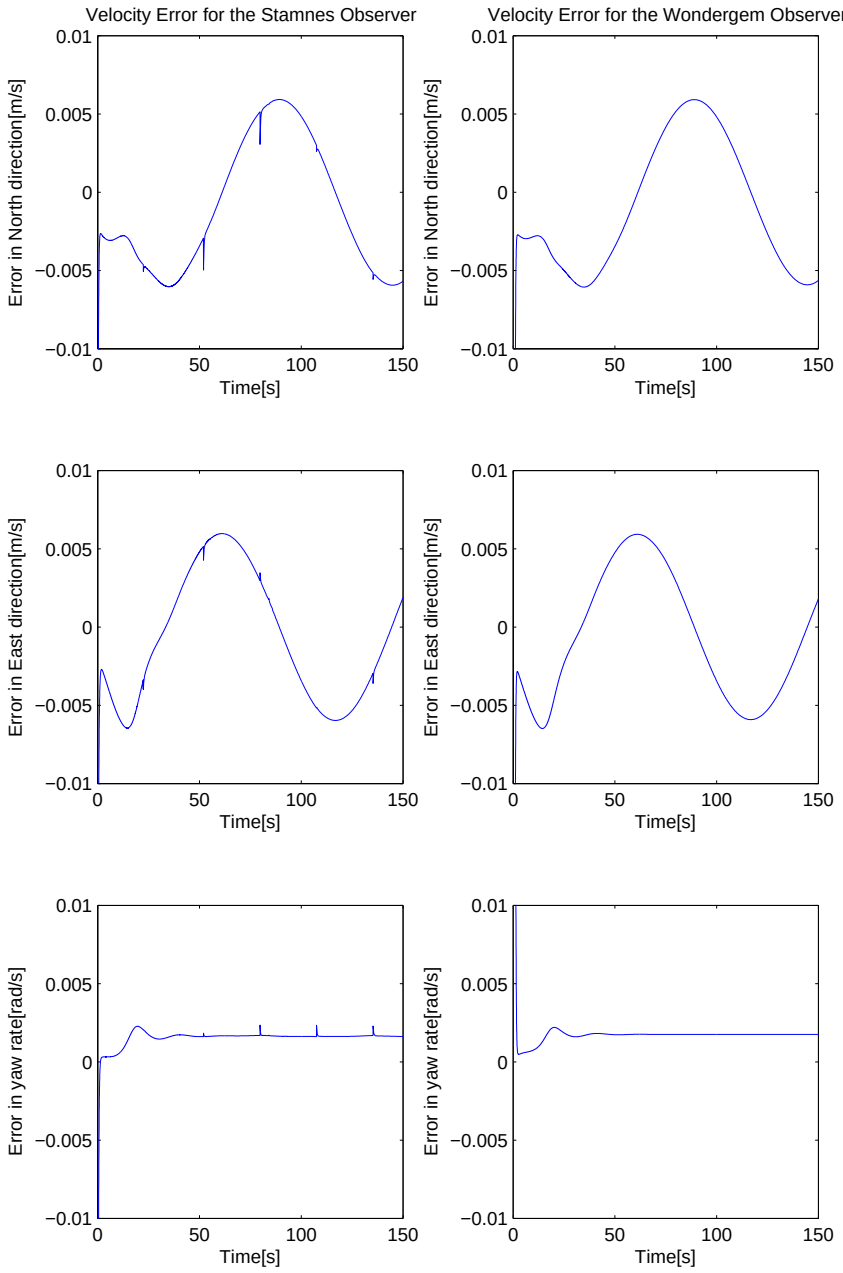

Figure 5.21: Case 4: Bias in observer ship model, circular path, observer velocity estimate error

Conclusion

The Stamnes Observer and the Wondergem Observer have successfully been implemented for a given ship model, and the properties of the two observers have been analysed and discussed.

Based on the analysis in Section 4.2, it can be concluded that the Stamnes Observer does not fulfill the requirements for uniform global asymptotical stability when used for the ship model. However, it is proven to be semi-globally uniformly exponentially stable, which causes both observers to have the same stability properties. The Stamnes Observer consists of equations of high complexity, making the implementation complicated. The opposite can be stated for the Wondergem Observer, which has a simpler mathematical structure. While both observers can achieve a satisfying result by tuning, the Stamnes Observer must be tuned carefully in order to avoid long run times during simulations, as discussed in Section 4.3.

The simulations in Chapter 5 show that the Wondergem Observer is slightly more robust to measurement noise or bias in the system equations, with regards to convergence time and lack of numerical inaccuracies. The run time when simulating on a standard desktop computer is one to two orders of magnitude less than for the Stamnes Observer. This observation can indicate that the Stamnes Observer is more difficult to implement in a realtime control system for this ship model.

Overall, a conclusion can be made that the Wondergem Observer is more robust, and simulates more efficiently than the Stamnes Observer. When it also is shown that the two observers have the same stability properties for the given ship model, the Wondergem Observer is to prefer both with regards to theoretical and practical aspects.

Further work

When implementing the observers in Matlab, no attempts have been done to optimize the code for improvement of run time. Also, while the observers have been simulated with measurement noise and model errors, the Stamnes Observer has not been tested for a physical model supply ship. Recommended further work is therefore to optimize the code in order to investigate if the run time for the Stamnes Observer can be reduced, and to test the Stamnes Observer with a model supply ship to verify the simulated results from this thesis.

Bibliography

O. Aamo, M. Arcak, T. Fossen, and P. Kokotovic. Global output tracking control of a class of euler-lagrange systems. In *Decision and Control, 2000. Proceedings of the 39th IEEE Conference on*, volume 3, pages 2478 –2483 vol.3, 2000. doi: 10.1109/CDC.2000.914174.

A. Astolfi, D. Karagiannis, and R. Ortega. *Nonlinear And Adaptive Control With Applications*. Communications and Control Engineering. Springer, 2008. ISBN 9781848000650. URL http://books.google.no/books?id=HYl1SCUpMccC.

A. Astolfi, R. Ortega, and A. Venkatraman. A globally exponentially convergent immersion and invariance speed observer for n degrees of freedom mechanical systems. In *Decision and Control, 2009 held jointly with the 2009 28th Chinese Control Conference. CDC/CCC 2009. Proceedings of the 48th IEEE Conference on*, pages 6508 –6513, dec. 2009. doi: 10.1109/CDC.2009.5399984.

A. Astolfi, R. Ortega, and A. Venkatraman. A globally exponentially convergent immersion and invariance speed observer for mechanical systems with non-holonomic constraints. *Automatica*, 46(1):182 – 189, 2010. ISSN 0005-1098. doi: 10.1016/j.automatica.2009.10.027. URL http://www.sciencedirect.com/science/article/pii/S0005109809004889.

T. Fossen. *Marine control systems: guidance, navigation and control of ships, rigs and underwater vehicles*. Marine Cybernetics, 2002. ISBN 9788292356005. URL http://books.google.no/books?id=B3ZwQgAACAAJ.

T. Fossen. *Handbook of Marine Craft Hydrodynamics and Motion Control*. John Wiley & Sons, 2011. ISBN 9781119991496. URL http://books.google.no/books?id=vCAzd3DaZCgC.

T. I. Fossen. *Nonlinear modelling and control of underwater vehicles*. PhD thesis, Norwegian University of Science and Technology, Department of Engineering Cybernetics, 1991.

H. Khalil. *Nonlinear Systems*. Prentice Hall, 2002. ISBN 9780130673893. URL http://books.google.no/books?id=t_d1QgAACAAJ.

E. Kreyszig. *Advanced Engineering Mathematics*. John Wiley, 2006. ISBN 9780471728979. URL http://books.google.no/books?id=3t7DQgAACAAJ.

M. Krstic. Nonlinear stabilization through long input delay #x2014;part i: Forward complete systems. In *Decision and Control, 2009 held jointly with the 2009 28th Chinese Control Conference. CDC/CCC 2009. Proceedings of the 48th IEEE Conference on*, pages 5245 –5250, dec. 2009. doi: 10.1109/CDC.2009.5399720.

K. Pettersen and H. Nijmeijer. Output feedback tracking control for ships. In H. Nijmeijer and T. Fossen, editors, *New Directions in nonlinear observer design*, volume 244 of *Lecture Notes in Control and Information Sciences*, pages 311–334. Springer Berlin / Heidelberg, 1999. ISBN 978-1-85233-134-4. URL http://dx.doi.org/10.1007/BFb0109933. 10.1007/BFb0109933.

R. Skjetne and H. Shim. A systematic nonlinear observer design for a class of euler-lagrange systems. 2001. URL http://med.ee.nd.edu/MED9/Papers/Nonlinear_control/Nonlinear_1/med01-118.pdf.

A. Stacey, 2010. Lecture notes in the class TMA4145-Linear Methods the autumn 2010, at NTNU, URL: http://www.math.ntnu.no/ stacey/documents/tma4145.lecture.beamer.2010-10-04.pdf.

F. White. *Fluid Mechanics*. Number v. 1 in McGraw-Hill Series in Mechanical Engineering. McGraw-Hill, 2003. ISBN 9780071215664. URL http://books.google.no/books?id=ZM2HPwAACAAJ.

M. Wondergem, E. Lefeber, K. Pettersen, and H. Nijmeijer. Output feedback tracking of ships. 2009. URL http://seweb.se.wtb.tue.nl/~lefeber/do_download_pdf.php?id=97.

M. Wondergem, E. Lefeber, K. Pettersen, and H. Nijmeijer. Output feedback tracking of ships. *Control Systems Technology, IEEE Transactions on*, 19(2):442 –448, march 2011. ISSN 1063-6536. doi: 10.1109/TCST.2010.2045654.

Øyvind Nistad Stamnes, O. M. Aamo, and G.-O. Kaasa. A constructive speed observer design for general euler–lagrange systems. *Automatica*, 47(10):2233 – 2238, 2011. ISSN 0005-1098. doi: 10.1016/j.automatica.2011.08.006. URL http://www.sciencedirect.com/science/article/pii/S0005109811003773.

Appendix A

User Guide to the Matlab Files

The Matlab files to be run is Main2.m, Main starts the simulation. If some tuning parameters are to be changed, this is done in both Main2.m and ship.m. This choise has been made in order to avoid global variables. The variables in Main2.m are used in Making_the_plots.m, and are neccesary to get correct plots. The variables in ship.m are the simulation variables, and give the actual results. The initial values are controlled from Main2.m.

All the other matlab functions are used accordingly to the system equations given in Chapter 3.